AN ABSTRACT OF THE THESIS OF

Sutara H. Suanda for the degree of Master of Science in Oceanography presented on December 11, 2009.

Title: Diurnal Wind-driven Processes on the Northern Monterey Bay Inner Shelf.

Abstract approved:

John A. Barth

In the summer of 2007, a biophysical experiment was conducted to identify physical processes that determine the delivery of invertebrate larvae and juvenile rockfish to rocky intertidal and kelp forest communities in northern Monterey Bay, California. The experiment was sponsored by the Partnership for Interdisciplinary Studies of Coastal Oceans (PISCO) and collected physical measurements including velocity from acoustic Doppler current profilers, surface gravity wave heights measured acoustically, and temperature from thermistor chain arrays both along- and across- the inner shelf in water depths of 10 – 60 m. The inner shelf is the transition between the nearshore and mid-shelf zones, and is defined where surface and bottom Ekman boundary layers overlap.

Previous work has shown that the inner shelf in this region is rich in physical processes across many space and time scales. The goal here is to identify and quantify the dominant processes at the diurnal (24 hour) period. Diurnal tides contribute less than 10% of the observed currents. Thus the focus is on the oceanic response to a strong (8 - 15 m/s daily maximum) along-shelf sea breeze which forces offshore

surface Ekman transport, drives average upwelling velocities of 26 m/day, and cools the water column 2 – 4^{o}/day. At 15 m (20 m) depth, measured diurnal surface transport is 36% ± 9% (77% ± 12%) of full theoretical Ekman transport. Examination of a diurnal heat budget shows that vertical advection is the dominant process during afternoon cooling (both horizontal advection and solar insolation are sources of heat during this period), and is needed to close the heat budget to within 5%. In contrast, during evening/early morning heating 92% of the observed heating is explained by along-shelf advection of a temperature gradient within the upwelling shadow, much greater than the heating attributed to either solar insolation (2%) or onshore motions (2%). Thus, the diurnal heat budget is closed to within a few percent and explained by two-dimensional processes: vertical advection by wind-driven upwelling during cooling and along-shelf advection during heating.

Diurnal Wind-driven Processes on the Northern Monterey Bay Inner Shelf

by

Sutara H. Suanda

A THESIS

submitted to

Oregon State University

in partial fulfillment of

the requirements for the

degree of

Master of Science

Presented December 11, 2009

Commencement June 2010

Master of Science thesis of Sutara Suanda
presented on December 11, 2009.

APPROVED:

Major Professor, representing Oceanography

Dean of the College of Oceanic and Atmospheric Sciences

Dean of the Graduate School

I understand that my thesis will become part of the permanent collection of Oregon State University libraries. My signature below authorizes release of my thesis to any reader upon request.

Sutara H. Suanda, Author

ACKNOWLEDGEMENTS

First and foremost, I would like to express sincere thanks to my advisor Jack Barth, without whom this work would have never come together. Jack has been a supportive advisor, providing direction and feedback at all points of this research. He has given me opportunities to explore both in the research necessary to complete this work as well as to pursue other opportunities outside of our department. He has also been a terrific cheerleader, motivating different aspects of the work, and urging me to think for myself. I would also like to thank the other members of my committee who read the thesis and provided feedback on the work. A large thank you goes to the PISCO field team and Brock Woodson who led the PISCO project which provided all the data for this thesis. I would like to thank my fellow graduate students and officemates who have been supportive with useful feedback and discussion as well as providing much needed distractions. Lastly, Kirsten deserves an entire bucket of thanks. She has been the most patient and supportive through this thesis writing adventure. It would not have been completed without her.

TABLE OF CONTENTS

TABLE OF CONTENTS (continued)

LIST OF FIGURES

LIST OF FIGURES (Continued)

LIST OF FIGURES (Continued)

LIST OF TABLES

LIST OF TABLES (Continued)

Introduction

This thesis presents an analysis based on observational data that describes the surface gravity wave, water column velocity, and thermal stratification response of the northern Monterey Bay inner shelf to forcing by diurnal sea breeze. This introduction sets the stage for the rest of the work by describing the relevance of examining sea breeze forcing to inner-shelf studies, the unique physical setting provided by northern Monterey Bay, as well as an outline of the thesis objectives and how I situate this work within the goals of the larger project that supported this research.

Dynamics and previous observational and modeling studies of the inner shelf

In northern hemisphere coastal regions, on the western (eastern) side of continents with strong equator (pole)-ward along-shelf winds, offshore surface Ekman transport drives upwelling of waters onto the continental shelf. The inner shelf is the region where shelf circulation adjusts to the presence of a coastal boundary (Lentz, 1994). It is formally defined to be the region outside of the surf-zone where surface and bottom Ekman boundary layers overlap (e.g. Lentz, 1994). It is also the region of active upwelling where a divergence of Ekman transport has been predicted, modeled, and observed (e.g. Mitchum and Clarke, 1986; Allen et al., 1995; Lentz, 1995; Lentz et al., 2001; Kirincich et al., 2005).

From a physical perspective, the inner shelf has eluded complete description because our understanding of the relevant forces in this region is incomplete. The momentum balance on the inner shelf involves frictional forces throughout the water column and often includes the effect of shoaling surface gravity waves (Lentz et al., 1999). It is historically under sampled as it presents a challenging work environment with water depths too shallow for full-size oceanographic research vessels. Even so, physical processes here are relevant to other fields of study as they play a role in the

dispersion and retention of nutrients, pollutants and invertebrate larvae, especially intertidal and kelp forest species (e.g. Farrell et al., 1991).

Previous observational studies of wind-driven inner-shelf circulation have focused on sub-tidal frequencies, thus expecting a steady Ekman balance in the momentum equations. Studies on the effect of along-shelf winds have documented the extent of Ekman transport divergence from its shutdown in shallow inshore waters to deeper offshore regions where full transport is realized (Lentz, 2001; Kirincich et al., 2005). Lentz (2001) found that on the Northern Carolina inner shelf the percentage of cross-shelf surface transport increased to the full theoretical value over a distance of 10km and that this result was sensitive to the level of stratification. Kirincich et al. (2005) found full theoretical surface transport realized at similar depths (~50 m) a closer distance to shore on the steeper Oregon inner shelf. This shows that water depth controls the region of Ekman divergence more so than distance to shore (Kirincich et al., 2005).

There are also observations that document the response of inner-shelf currents to cross-shelf wind forcing (e.g. Fewings et al., 2008). Fewings et al. (2008) found that cross-shelf exchange was better correlated with cross-shelf than along-shelf winds on the Martha's Vineyard Coastal Observatory inner shelf. While Ekman transport shuts down as the shore is approached, currents driven by cross-shelf winds can be more effective as they do not experience the same divergence (Tilburg, 2003).

In two previous modeling studies of the inner-shelf response to wind forcing (Tilburg, 2003; Austin and Lentz, 2002), the inner shelf becomes unstratified due to either offshore movement of the upwelling front during sustained upwelling or due to convective instability during downwelling. While increased stratification limits the vertical extent of turbulent eddies allowing mass and momentum to be more efficiently mixed in a shallow surface layer, destratification has an adverse effect on wind-driven transport efficiency. Related to stratification, cross-shelf circulation on the inner shelf has also been shown to be sensitive to the form of eddy viscosity (Lentz, 1995). A swift approach to steady state Ekman balance can be achieved with

an eddy viscosity profile that increases linearly from the ocean surface (Madsen, 1977). Thus, if inner-shelf regions remain stratified along-shelf winds could still be an effective mechanism at driving transport.

Finally, a recent development in understanding cross-shelf motions on the inner shelf is to include the effect of shoaling surface gravity waves. On the Northern Carolina inner shelf Lentz et al. (1999) identified gradients in the cross shelf wave radiation stress to be important in the momentum balance. In a further study, wave-driven cross-shelf circulation was consistent with a balance between the Coriolis force and the Hasselman wave stress resulting in surface velocities comparable to those driven by the wind (Lentz et al., 2008). Though this additional source of offshore motion did not significantly alter Ekman transport percentages on the Oregon inner shelf, Kirincich et al. (2008) also found consistent results, showing the importance of surface gravity wave forcing on the inner shelf. At a Monterey Bay location, a recent study found that diurnal sea breeze significantly altered cross-shelf current profiles through both direct cross-shelf wind forcing and surface gravity wave forcing (Hendrickson and MacMahan, 2009). They found that the Monterey Bay sea breeze increased wave heights by 20%, and that diurnal increases in surface stress and surface gravity wave forcing can have a similar effect on inner-shelf current profiles on the diurnal timescale as on subtidal ones reported by Fewings et al. (2008) (Hendrickson and MacMahan, 2009).

Physical setting of Monterey Bay

Monterey Bay is a large semi-circular bay situated in Central California. Like much of the West Coast of North America, it is subject to upwelling-favorable winds for a portion of the year, particularly in summer. The regional-scale, summer-time oceanic circulation in the bay has been the subject of many studies (Rosenfeld et al., 1994) and is still an active area of research due to the unique and complicating effects

bay geometry and bathymetric features have on oceanic circulation (e.g. Ramp et al., 2005; Rosenfeld et al., 2008).

During sustained upwelling-favorable winds, the main coastal upwelling center is to the north of the bay at Pt. Ano Nuevo (Rosenfeld et al., 1994). Cold upwelled waters can be seen in satellite imagery to travel both across the mouth of Monterey Bay and offshore, isolating bay waters from regional-scale circulation (Figure 1) (Rosenfeld et al., 1994; Paduan and Rosenfeld, 1996). Bay waters onshore of the upwelling jet are shielded from regional wind by the Santa Cruz mountains, and form a recirculation zone in the northern part of the bay (Rosenfeld et al., 1994; Graham and Largier, 1997). This region is part of a counter-clockwise rotating gyre characterized by cold subsurface water capped by a 5 - 10 m surface layer of water warmed by solar insulation termed the 'upwelling shadow' (e.g. Rosenfeld et al., 1994; Graham and Largier, 1997; Ramp et al., 2005).

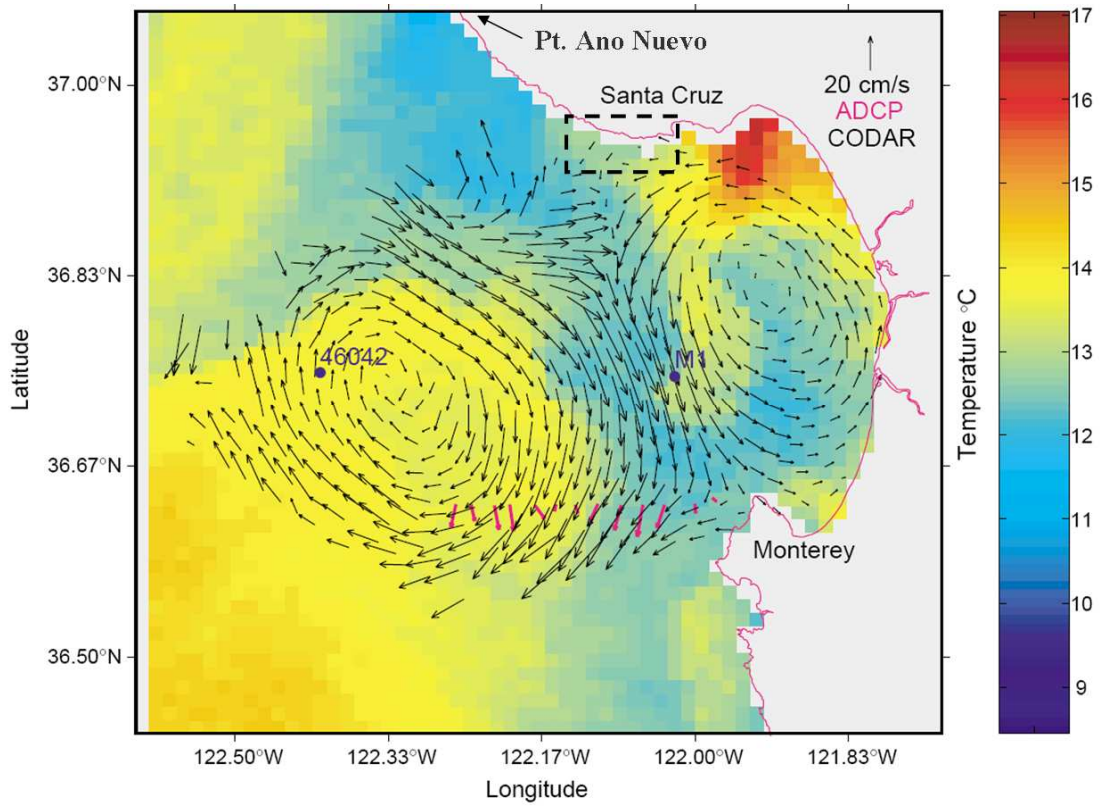

Figure 1.

Figure 1. Daily-averaged surface currents from CODAR and SST from AVHRR for Monterey Bay during upwelling. Dotted box denotes location of current study. Pt. Ano Nuevo upwelling center is to the North. Figure reproduced from Paduan and Rosenfeld (1996).

From a biological perspective, the upwelling shadow region has been observed to be more turbid than offshore upwelling jet waters with lower nutrient content and higher chlorophyll levels (Graham and Largier, 1997). Elevated primary production in a confined region increases food availability for higher trophic level organisms and the recirculation can also be conducive for larval retention.

The frontal region separating the shadow from offshore upwelled waters behaves as a buoyant front further inhibiting exchange and reinforcing the recirculation (Graham and Largier, 1997; Woodson et al., 2009 *in press*). The inner shelf study area of this thesis is within this frontal region. Woodson et al. (2009) report that in the along-shelf direction this front is subject to buoyant forcing due to the temperature difference between the upwelling shadow and offshore upwelling jet, an along-shelf pressure gradient resulting from the sea level difference between the shadow and Pt. Ano Nuevo upwelling center, as well as modulation from the diurnal sea breeze.

Local forcing and sea breeze

Because of effective shielding from regional forcing, recent work on the northern Monterey bay inner shelf has shown local processes (e.g sea breeze winds) to be important (Drake et al., 2005; Woodson et al., 2007; Woodson et al., 2009 in press). On seasonal timescales, currents in the northern bay more closely correlate to a local wind station than to the offshore NDBC buoy 46042 which is more representative of regional winds (Drake et al., 2005). The sea breeze wind is oriented predominantly alongshore and Woodson et al. (2007) find diurnal upwelling to result in water column cooling up to 5 ^{o}C occurring at midday when solar heating is strongest (Woodson et al., 2007).

Sea breezes are a common feature of mid-latitude coastal areas. The atmospheric sea breeze circulation results from daily differential heating of land and

sea. For the particular case of Monterey Bay, a few topographic characteristics make this forcing particularly potent. The Salinas river valley to the east of Monterey Bay is a wide expanse of land that is subject to intense heating in the summer and the Santa Cruz and Gabilan mountain ranges funnel sea breeze winds into this valley (Banta et al., 1993). More recently, the increase in strength of diurnal wind power over Monterey Bay has also been reproduced by the Navy's COAMPS model as noted in (Kindle et al., 2002).

Heat Balance

Previous studies have used experimental data to examine heat balances over the continental shelf, and compare contributions of various terms to the observed mean or fluctuating heat content. The Coastal Ocean Dynamics Experiment (CODE) region (centered on 38.5^{o}N, 123.5^{o}W) has achieved considerable attention with multiple field programs over the last 30 years. Lentz (1987) writes a conservation equation for the heat content of a 3-dimensional volume extending 56 km along-shelf, 25 km across-shelf and from the surface to the bottom during the summer upwelling season. Lentz (1987) finds good agreement with measured offshore heat flux and a 2-dimensional Ekman model across the control volume. The study also closed both the mean and subtidal fluctuating heat budgets. Turning attention towards the winter and spring seasons, Dever and Lentz (1994) estimate the heat balance for a 2-dimensional cross-shelf slice in this region. The balances in the subtidal fluctuating heat budgets are found to be similar to the summer season, but the mean heat balance showed the importance of 3-dimensional processes during the winter period (Dever and Lentz, 1994).

With the purpose of identifying dominant processes responsible for upper water column warming in response to wind relaxation during the Coastal Ocean Dynamics Experiment (CODE), Send et al. (1987) use a conservation equation written for the heat content within a surface layer. This approach was successful as each term

in the conservation equation was evaluated with data, giving insight to the relative size of various contributions. With a focus on subtidal timescales, Send et al. (1987) find that surface heating and alongshelf advection are the largest contributors to observed warming in the CODE region.

Motivation and objectives for thesis

This work is part of the Partnership for Interdisciplinary Studies of Coastal Oceans (PISCO) 2007 summer study in northern Monterey Bay. The larger goal of this study was to determine the physical processes that control the recruitment of marine invertebrates and juvenile fishes to the area. The interaction of the upwelling shadow with other physical forcing mechanisms provides the setting for this work and many processes spanning a variety of frequencies have the potential to affect recruitment of organisms.

The focus of this thesis is on forcing mechanisms in the diurnal frequency band. The driving questions here are: What processes are responsible for the observed daily heating and cooling on the inner shelf? What percentage of Ekman transport can be expected with diurnal period along-shelf forcing? Is the mechanism of Stokes' drift important for cross-shelf exchange in this location? By the end, I will have a census of forcing mechanisms in this frequency band, be able to determine the relative strength of the different forces, and provide insight into their role in retention and delivery of rocky intertidal organisms.

The rest of the thesis is organized as follows: The methodology chapter describes the analysis procedures. The results chapter quantifies the relation between diurnal forcing mechanisms and observed currents, compares theoretical to measured transports, evaluates the contributions of Stokes' drift and presents the results of a diurnal heat balance. The discussion chapter is a closer look at the results, an interpretation of their implications, and a description of future work. Lastly, results are summarized in a brief conclusions chapter.

Data and Methods

This chapter is divided into 3 sections. The first describes data sources and instrumentation used in this study along with initial processing procedures. The second section describes the statistical techniques including spectral, and correlation procedures along with regression techniques, the criteria and procedure for creating a canonical wind-day, as well as the way effective degrees of freedom are estimated. The last section of this chapter describes methods to extract various signals from data. This includes estimation and removal of tides, estimates of cross-shelf transport from current profiles and calculation of theoretical Ekman transport. It also presents the derivation of the heat budget equation, how individual terms are estimated, and the uncertainty associated with these estimates.

Instrumentation and Data Sources

Field observations used in this thesis are from data collected by the 2007 PISCO summer study in northern Monterey Bay. Water-column velocity and temperature data are from a series of inner-shelf arrays described by Woodson et al. (2009). Though the PISCO study instrumented a 15-km stretch of the northern Monterey Bay inner shelf and included moorings, Acrobat tows, and biological sampling, the description below focuses only on moored data used in this thesis.

Moorings were placed in cross-shelf arrays at the 10-m, 20-m, 30-m, and 60-m isobaths off Terrace Point (TPT), Sand Hill Bluff (SBH), and Light House Point (LHP) (Figure 2). Temperature was recorded from May – September 2007 with loggers (Onset, Inc.) on each mooring recording temperature every 2 minutes (Stowaway Tidbits), or every 30 seconds (XTIs) (Woodson et al., 2009). Temperature loggers at the surface recorded at 4 min intervals.

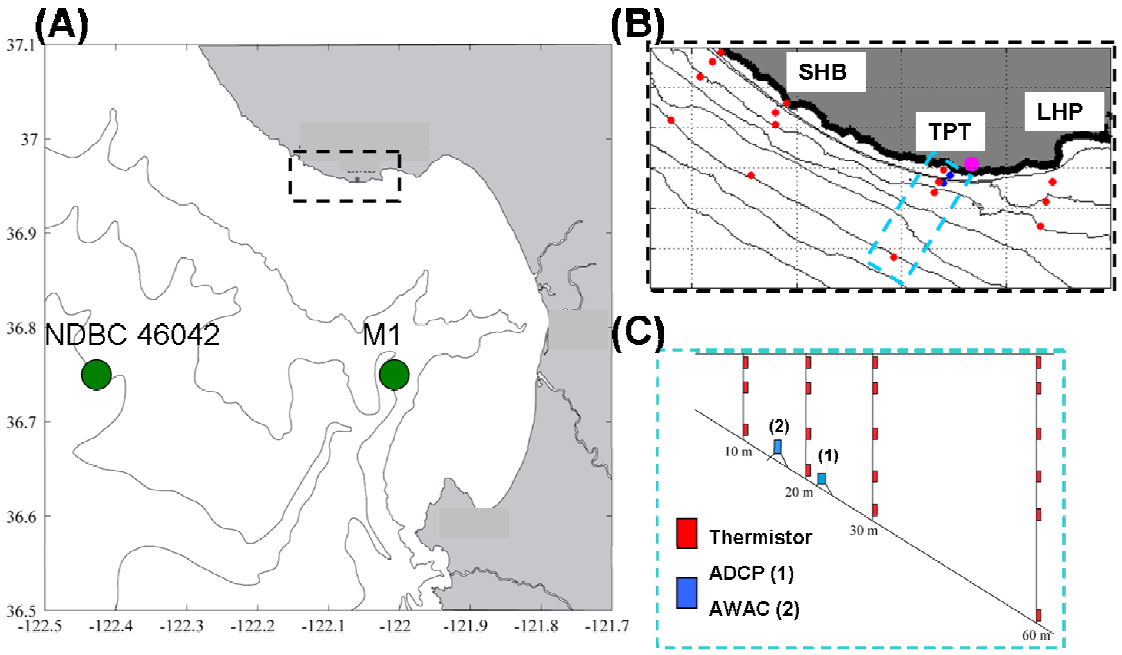

Figure 2: (A) Map of Monterey Bay showing location of offshore wind stations NOAA NDBC 46042 and MBARI M1 (map courtesy C.B. Woodson). The study location is denoted by a dotted square. (B) Close-up of inner-shelf study region. Bathymetry is shown in 10-m increments along with thermistor chains (red dots) and acoustic current profiler (blue dot) locations. Also noted is the location of UCSC Long Marine Lab (purple dot). (C) Cross-shelf view of thermistor and current profiler array off of Terrace Point (TPT).

Two and four minute temperature data were run through a three standard deviation filter to remove outliers beyond three standard deviations of the mean for each instrument and bin-averaged into hourly time series. For the first few weeks of deployment, the surface temperature from the 10-m TPT mooring showed values equal to or lower than the 5-m logger on the same mooring. These values were separated by a data gap and followed by more realistic readings of surface waters warmer than the 5-m logger. I considered the initial values suspect and did not include them in the analysis. Data was also missing over the last few weeks of the deployment from the bottom temperature logger at the TPT 20-m mooring.

At Terrace Point, an Acoustic Doppler Current Profiler (ADCP; RDI Workhorse 600 kHz, Teledyne Inc.) was deployed at the 20-m isobath. The ADCP

recorded 45 pings per 2-minute ensemble averaged into 1-m bins. A second instrument, an Acoustic Wave and Current Profiler (AWAC; Nortek 1 MHz) was deployed nearby (15-m isobath). The AWAC was programmed to sample water column velocity profiles for 40 minutes of every hour using 2-minute ensembles of 40 pings. The instrument collected 2-Hz acoustic surface tracking (AST) during the remaining 20 minutes. This AST record combined with bottom pressure and wave orbital velocity measurements allow the AWAC to resolve the surface gravity wave directional spectrum. Current profiles from the AWAC were averaged into 0.5-m bins. Though the ADCP was deployed for the entire summer study (May – September 2007), the AWAC was only deployed for the month of July, 2007. Wave data gathered by the AWAC was compared and supplemented with directional wave data made available through NOAA National Data Buoy Center (NDBC) number 46042.

With acoustically measured currents, near the surface up to 10% of the water column can be contaminated by side-lobe reflection. To minimize data loss a “tide-following” processing method is adopted to preserve as much of the velocity profile at a given hour. With the AWAC, accurate measurements of the surface are made by both acoustic surface tracking and a bottom pressure sensor. Hourly-averaged pressure measurements are used to identify the surface and all velocity data above and 10% below this level are discarded. The RDI ADCP has no pressure sensor, so to find the surface the tide-following method of Kirincich et al. (2005) is used. Backscatter intensity from the 4 beams are added together and the maximum value is taken as the surface. Again, all velocity data above and 10% below this level are discarded. Both sets of 2 minute current measurements are averaged to hourly values.

Measured water-column velocities are rotated into the principal axes as derived by the hourly depth-averaged values. The principal axes is such that variance is maximized along the major axis and minimized along the minor axis. Once rotated, currents were assumed to be in the along (across) shelf direction for the major (minor) axes.

Wind data were taken from a variety of sources to complement *in situ* measurements. In this thesis, the term “regional” winds are taken from Monterey Bay Aquarium Research Institute (MBARI) M1 mooring, and NOAA buoy 46042. In addition, “local” wind data are taken from UCSC Long Marine Lab, less than 2 km from the TPT inner-shelf array.

Aside from the initial wind calculation (Section 1, Results), a typical west-coast coordinate system of positive y-axis along-shelf towards the pole, and x-axis positive onshore with zero at the coast is used in all analysis to follow.

Statistical Tools

In each Results section, after reporting the mean and standard deviations of wind speed, on/offshore current component, and temperature measurements, power spectral density plots are presented. In the frequency domain, the calculated power spectra (*S*) show the distribution of variance in a time series across frequencies ranging from the mean to the Nyquist frequency.

$$S(f_k) = \frac{1}{N\Delta t}\left[X^*(f_k)X\ (f_k)\right], \quad k = 0, 1, 2, \ldots, N-1$$

X = Fourier transform of time series x(t)

X^* = Complex conjugate of $X(f)$.

N = Number of samples

Δt = sample interval

Prior to calculating power spectra, the mean of all time series are removed. Time series are multiplied by a triangle window to minimize data edge effects and calculated to have 20 degrees of freedom by band averaging neighboring frequencies. The reported spectra are also variance-preserving by multiplying calculated spectra by

the ratio of the variance of the original time series divided by the variance of the triangle-windowed time series.

Cross-correlation analysis is used to quantify the relationship between two variables. The correlation coefficient (CC) is defined as the covariance of two random variables divided by the product of their standard deviations (Emery and Thompson, 1997).

The Monterey Bay sea breeze is intermittent in time. Analysis in the frequency domain applied across an entire observation period is indiscriminant of whether or not this forcing is present throughout the period. The time-varying amplitude of frequency constituents in a time series can be followed by a windowed Fourier transform or complex demodulation (e.g. Rosenfeld, 1988). Although wind and water velocity time series were complex demodulated at the diurnal period, such analyses is not reported as the cross-correlation is sufficient to demonstrate the relationships in this study.

In this study both standard linear and neutral regression are used according to the model;

$$Y = mX + b$$

With this linear model, the slope (m) is used to quantify the percentage of a model signal (X) that is explained by an external process (Y). Standard linear regression minimizes variance in one dimension, thus assuming that the model (X) is error free. Linear regression is used to transform offshore significant wave heights to inner-shelf wave heights (Stokes' drift section, Results) and to compare contributions of heat flux terms to an observed amount of heating (heat budget section, Results).

The neutral regression technique used follows Garrett and Petrie (1981) as in Kirincich et al (2005). For relating two variables that both have measured uncertainties, neutral regression fits a straight line through data by minimizing the variance in both x- and y- directions. If measurement uncertainties are not known, the

slope of the regression line is defined as the square root of the variance ratio between the two time series:

$$m = \left(\frac{\sigma_X^2}{\sigma_Y^2} \right)$$

One goal here is to quantify the effects of a strong diurnal sea breeze on the circulation and temperature structure of the inner shelf. A way this is done is by creating a canonical sea breeze day. Over the 2.5 months when all data were available, days when local westerly sea breeze reached a maximum of at least 8 m/s are averaged together. There are 45 such days during this study (Figure 3). Hourly values of wind, surface gravity wave, temperature, and velocity at each level in the water column, are averaged in time centered on the peak of the westerly wind. The 12 hours leading to and following maximum wind are also averaged, thus a picture of the canonical wind-forced day is formed.

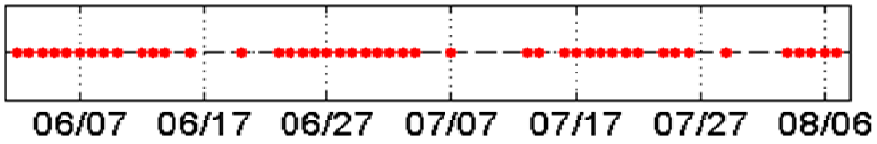

Figure 3: Timeline marking 45 days (red circles) used in creating ensemble-averaged canonical day. The x-axis marks the date (mm/dd)

In all measurements used here, the effective degrees of freedom are less than if each observation were statistically independent. This effects the degree of significance in correlation coefficients as well as the size of confidence intervals on both linear and neutral regression coefficients. As will be shown, a large percentage of variance in all hourly time series was found in the diurnal band, indicating an integral timescale of 1 day. Thus, the number of degrees of freedom were estimated for all time series by

assuming that each day (24 hour interval) was an independent observation. With this criteria, the AWAC deployment had 27 effective degrees of freedom, the longer ADCP deployment and wind measurements had over 100 effective degrees of freedom, and variables ensemble-averaged in the canonical day had 45 effective degrees of freedom. All correlation coefficients reported in the text will be significant at the 95% level unless otherwise noted. Confidence intervals for regression slopes and intercepts will also be reported at the 95% level.

The diurnal frequency band is the primary interest of this thesis and for Ekman transport estimates data are low-pass filtered using a Cosine-Lanczos filter as in Mooers (1968). The filter is implemented with a 20-hour filter cut off. The low-passed time series will retain less than 1% of the power at the semidiurnal frequency while preserving about 70% of the power in the diurnal band.

Estimating Signals from Data

Tides

Harmonic tidal analysis on measured currents, bottom pressure, and temperature is conducted with T_TIDE, a package of programs for MATLAB that performs least squares harmonic analysis on scalar and vector time series (Pawlowicz et al., 2002). As will be shown in Results, in contrast to surface tides being predominantly semidiurnal on the US west coast (e.g. Rosenfeld et al., 2008), harmonic tidal analysis on depth-averaged currents estimate diurnal tidal velocity to be larger than the semidiurnal. Rosenfeld et al (2008) attribute this to leakage from sea breeze wind-driven currents into diurnal tidal frequencies at this location. On the other hand, semidiurnal surface tidal velocity from harmonic analysis is more reliable as it is not subject to leakage from diurnal wind and compares well with previous results (Rosenfeld et al., 2008).

To create a canonical wind-driven day it is necessary to account for and remove, the diurnal tidal signal. As the amplitude of diurnal tidal velocity from harmonic analysis is unreliable, instead it is estimated from a ratio between the expressions for sea level and depth-averaged velocity from solving the shallow-water equations applied to frictionless channel with tidal forcing (Gill, 1982) and assuming that this ratio remains the same regardless of tidal frequency.

$$V_{K1} = \frac{BP_{K1} \times \omega_{K1}}{BP_{M2} \times \omega_{M2}} V_{M2}$$

V_{M2} = M2 tidal velocity

V_{K1} = K1 tidal velocity

BP_{K1} = K1 tidal bottom pressure

BP_{M2} = M2 tidal bottom pressure

ω_{K1} = K1 tidal frequency

ω_{M2} = M2 tidal frequency

Amplitudes of tidal velocities can change with time and complex demodulation provides a measure of the time-varying amplitude of a sinusoid. Thus, instead of using the harmonic amplitude of depth-averaged M2 velocity (0.035 m/s) to predict the K1, the mean of the demodulated M2 amplitude is used (0.053 m/s). A synthetic sinusoidal K1 velocity time series is created with amplitude estimated with above ratio (0.022 m/s) and phase from the T_TIDE analysis and subtracted from velocity data prior to constructing the canonical day.

The local Coriolis acceleration can be modified by either lateral density gradients as in Mooers (1975), or by the vorticity of low-frequency currents (Lerczak et al., 2001), effectively stretching or contracting the internal wave pass-band. However, for this study the diurnal frequency is assumed to be below the internal wave pass-band such that the diurnal tides do not have vertical structure and are

completely contained within depth-averaged velocities. Depth-averaged velocity is removed prior to the analysis of diurnal wind-driven currents. Monterey Bay is well-known to have energetic semidiurnal baroclinic tides associated with the Monterey submarine canyon (e.g Petruncio et al., 1998). Depth-dependent velocities are low-pass filtered (Mooers, 1968) to preserve frequencies lower than 1/20 cph prior to wind-driven current analysis.

Surface stress, and theoretical and measured transport

Estimates of surface stress acting on the ocean are made from the Long Marine Lab wind measurements using the bulk formula of Large and Pond (1981) assuming a neutrally stable atmosphere. The along-shelf wind stress is calculated as:

$$\tau_s^y = \rho_a C_d |V|^2$$

ρ_a = density of air (1.2 kg m^{-3})
C_d = linear drag coefficient (s m)$^{-1}$
V = wind speed at 10 m (m s^{-1})

The theoretical Ekman transport estimate is made assuming a steady, linear along-shelf momentum equation with no bottom stresses or pressure gradients. In this case the depth-integrated balance in the cross-shelf direction is:

$$U_E = \frac{\tau_s^y}{\rho_o f}$$

ρ_o = mean water density (1025 kg m^{-3})
f = local Coriolis parameter (8.78 x 10^{-4} s^{-1})
U_e = surface Ekman transport (m^2 s^{-1})

Though the diurnal wind that is the focus of this study is not steady, measured surface transports are compared with the full theoretical value as in previous studies so a comparison can be made (Lentz, 2001; Kirincich et al., 2005). Furthermore, the theoretical value provides an upper bound for the amount of cross-shelf transport that can be driven by along-shelf winds (Woodson et al., 2007; Kirincich et al., 2005). Surface layer transports are extracted from velocity profiles following Kirincich et al (2005). Hourly values of cross-shelf, depth-dependent velocity are integrated from the first zero crossing to the shallowest good bin. As the upper 10% of the water column is excluded due to surface side-lobe reflection, velocity profiles need to be extrapolated to the surface to avoid under estimating the transport. Two extrapolation techniques are considered here. The first is a slab extrapolation to the surface where a constant velocity between the last good near-surface velocity and the actual surface is used. The second method linearly extrapolates the velocity profile from the two highest measurements to the surface assuming a constant velocity slope (Figure 4).

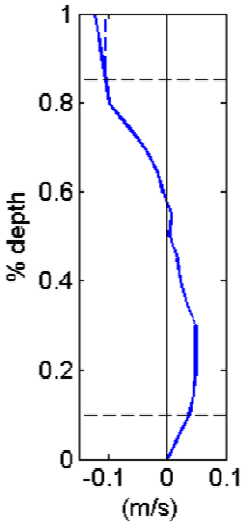

Figure 4: Example of current profile with both linear (solid) and slab (dashed) extrapolations from shallowest good bin to surface and interpolation from the deepest bin value to 0 at the bed. Horizontal dashed lines mark the locations in the water column where extrapolation (interpolation) begins.

Stokes' Drift

Beginning with the observational study of Lentz et al. (2008), cross-shelf wave-driven circulation on the inner shelf has been quantified by two methods. The first is the correlation between subtidal theoretical depth-averaged offshore velocity due to an Eulerian return flow (U_{st}) and observed subtidal depth-averaged offshore velocity. The second is to examine cross-shelf current profiles for expected dynamics. Only the first method is used and described here as this mechanism does not appear to be a significant source of cross-shelf motion at this location.

Following Lentz et al. (2008), Stokes' mass transport due to shoaling linear surface gravity waves is written as:

$$Q_w \approx \frac{gH_{sig}^2}{16c}\cos(\theta_w) = -U_{st}h$$

Q_w = onshore mass transport ($m^2\ s^{-1}$)
g = gravitational acceleration (9.81 $m\ s^{-2}$)
H_{sig} = significant wave height (m)
c = shallow water wave speed ($m\ s^{-1}$)
U_{st} = depth averaged offshore velocity ($m\ s^{-1}$)
h = water depth (m)
θ_w = incoming wave angle (^{o})

In our study area, the AWAC measured both significant wave heights and mean wave direction for the month of July, 2007. However, to encompass events where offshore significant wave height increased above 3 m, a longer time series was desired. Kirincich et al. (2008) successfully transformed wave heights measured offshore to inner-shelf locations in central Oregon with linear regression. The wave height time series at Terrace Point was lengthened in a similar fashion by linear regression of NDBC wave heights. A further simplification was made by assuming waves arrived

shore normal, a reasonable approximation given the AWAC mean wave direction was oriented perpendicular to shore most of the time.

Heat Budget

The heat budget calculation here follows Send et al (1987). The purpose is to compare the relative importance of various terms in a conservation equation written for the heat content within a well-mixed surface layer. In this study, heat content (H) is calculated for the upper 5 meters of water at the TPT 20-m thermistor chain. This can be written:

$$H = \int_{-5}^{0} \rho_o C_p (T - 11°C) dz$$

H = Heat content (J m^{-2})
ρ_o = Mean water density (1025 kg m^{-3})
C_p = Specific heat (3993 J (kg $^oC)^{-1}$)
T = Temperature of layer (^oC)

A positive heat content is defined for temperatures above 11^{o}C, the average value of the daily low temperature at the bottom thermistor. The integral is written in finite difference form:

$$H = (2.5m)\rho_o C_p \sum_{n=1}^{2} (T_n - 11°C)$$

where the index (n) is the surface (n = 1) and 5-m thermistor (n = 2).

To develop the heat budget equation for H, we begin with writing the conservation of thermal energy equation:

$$\rho_o C_p \left(\frac{\partial T}{\partial t} + \frac{\partial (uT)}{\partial x} + \frac{\partial (vT)}{\partial y} + \frac{\partial (wT)}{\partial z} \right) = \frac{\partial Q}{\partial z} + F_z$$

Where the material change in temperature is expressed as the sum of local temperature change with advective fluxes in three dimensions. This is equal to the sources and sinks of heat which are the vertical flux divergence of incoming solar energy (Q) and turbulent diffusion. The vertical component of the turbulent flux (F_z), orders of magnitude higher than the horizontal components, is the only one considered potentially important. However, next we integrate this equation over the upper 5 m of the water column. In the Send et al (1987) formulation, integration is to a level below a well-defined surface mixed-layer, excluding possible effects of vertical entrainment through wind-generated mixing. At our inner-shelf location, there is no such well-defined mixed-layer. Instead 5-m is used as the layer depth because it is below a mixed-layer and we further assume that solar heating effects are confined to this layer. Lastly, temperature measurements were available at this depth, leaving no need to choose an arbitrary layer depth.

The integrated equation becomes:

$$\rho_o C_p \left[\int_{-5}^{0} \left(\frac{\partial T}{\partial t} + \frac{\partial (uT)}{\partial x} + \frac{\partial (vT)}{\partial y} \right) dz + w_{(-5)} T_{(-5)} \right] = Q_{(0)}$$

Next, invoking the continuity principle, assuming slab motions where the horizontal velocities are constant across the 5 m layer, and subtracting the reference temperature we can write a simplified form of the material change in H, reorganized so that it is expressed in terms of the observed local rate of change of H. This leaves us with a

conservation equation whose balance between the right-hand and left-hand side can be tested.

$$\frac{\partial H}{\partial t} = Q - u\frac{\partial H}{\partial x} - v\frac{\partial H}{\partial y} - w_{(-5)}\rho Cp(T_{(-5)} - T_{ref})$$

From here on the subscript (0) has been dropped from the heat flux (Q) with the understanding that it is the surface value. Absent from the above formulation is the entrainment flux due to turbulence. A balance in the above equation and analysis of Richardson numbers will support this simplified formulation.

In this work, Q is further simplified to consist entirely of incoming shortwave solar radiation measured at MBARI M1 mooring as local measurements from Long Marine Lab were unavailable due to sensor malfunction. The uncertainty associated with the simplification made to net surface heat flux (Q) is discussed at the end of this section.

Terms in the above equation that involve partial spatial derivatives are estimated directly from data by finite centered difference (Figure 5). The heat flux magnitude (Q), velocity (u, v) and integrated heat content (H) used in the equation are taken from hourly values.

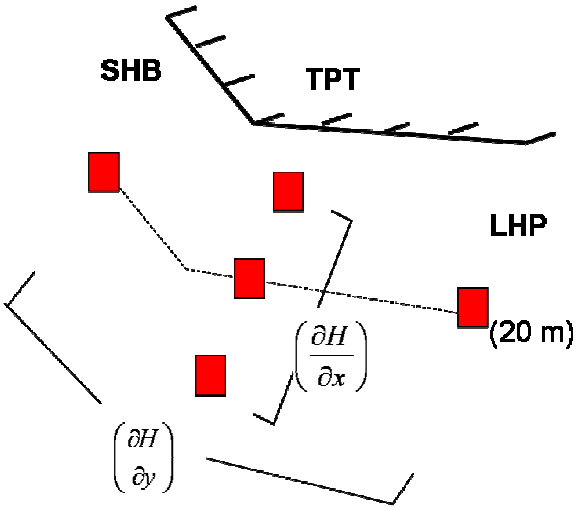

Figure 5: Schematic of centered finite differences used to calculate spatial derivatives. Red squares denote thermistor chain locations used and the dotted line is the 20-m isobath.

Results from this analysis are presented in two locations. The first is an attempt to explain heating periods over a 4-day time series (Heat budget section, Results). The second is within the canonical day description where it is used to explain both heating and cooling periods. The heating period only involves the first three terms on the left hand side of the above conservation equation. The cooling period requires the final vertical advection term ($w_{(-5)}\rho C_p(T_{(-5)} - T_{ref})$).

Vertical velocities are not measured directly and instead are inferred in two ways. The first is from the displacement in time of isopycnals assuming no mixing. The second is from an assumption of 2-dimensionality with no along-shelf variations. The 2-dimensional continuity equation is written as:

$$\frac{\partial u}{\partial x} + \frac{\partial w}{\partial z} = 0$$

Integrating this equation horizontally from an onshore location with no cross-shelf velocity to the instrument location and vertically integrating from the zero-crossing in

cross-shelf velocity to the surface, measured offshore (negative) surface transport during the cooling period should equal the positive vertical flux of mass through a horizontal plane (upwelling):

$$w = \frac{-U_s}{L}$$

w = Vertical upwelling velocity (m s^{-1})
U_s = Cross-shelf surface transport (m^2 s^{-1})
L = Length of upwelling region (m)

Richardson number

The bulk Richardson number is defined to be the ratio of the square of the buoyancy frequency to the square of velocity shear:

$$Ri = N^2\left[\left(\frac{\partial u}{\partial z}\right)^2 + \left(\frac{\partial v}{\partial z}\right)^2\right]^{-1}$$

Where N^2 is the square of the buoyancy frequency defined as:

$$N^2 = -\frac{g}{\rho_o}\frac{\partial \rho}{\partial z}$$

In this work, density is assumed to be a linear function of temperature at constant salinity. During this study the standard deviation of measured salinity derived

from 21 CTD casts was only 0.05 psu, and salinity variations are assumed to have a negligible effect on density.

The Richardson number was calculated for both hourly values of the entire record as well as for the canonical wind day. With the terms written as finite centered differences, ADCP currents and thermistors from the 20-m mooring provide estimates of the Richardson number at 3 different levels of the water column (Figure 6).

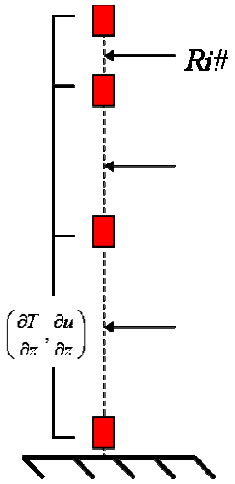

Figure 6: Schematic of thermistor chain at TPT 20-m showing three locations where the Richardson number is estimated with this data.

Estimating uncertainties

Signals estimated from observational data come with associated uncertainty due to measurement errors or errors from the difference between methods chosen to derive a particular quantity. These uncertainties propagate through calculations and determine the level of confidence in results. The discussion here focuses on the uncertainty in estimating various terms in the diurnal heat balance.

Measurement errors exist for both temperature and velocity as neither temperature loggers nor acoustic current profilers have perfect accuracy. Each individual measurement with a Stowaway logger has an error of 0.4^{o} C due to

instrument accuracy. The configuration of the RDI ADCP gives a velocity error of 0.5 cm/s for each 2 minute ensemble. Both hourly averaging, and ensemble averaging to create the canonical day decreases these errors by 1/sqrt(N) (N = 30 for hourly averages and N = 45 for canonical day). The associated measurement error in the hourly canonical day is about 1% for both heat content (*H*) and horizontal velocities (*u, v*).

A further source of error comes from the assumption of along-shelf uniformity used to estimate the upwelling velocity (*w*). Along-shelf velocities measured at SHB are used in conjunction with the those at TPT to estimate the along-shelf velocity gradient ($\partial v / \partial y$) resulting in deviations of 5% from the 2-D approximation. A larger source of error comes from determining the principal axis of rotation using hourly depth-averaged currents. A 2^o difference in principal axis is found if low-pass filtered depth-averaged currents are used instead. This results in about a 25% uncertainty in the estimate of cross-shelf transport, which also influences estimated upwelling velocities as well as the length of the region of active upwelling.

The estimate of heat flux (*Q)* here ignores the contributions of heat exchange with the atmosphere through sensible and latent heat as well as the constant heat loss due to long wave radiation. CODE measurements of coastal ocean heat flux near this latitude found that combined heat loss to the atmosphere was approximately constant throughout the day (~ 60 W m^{-2}), an order of magnitude smaller than incoming shortwave radiation (Rosenfeld, 1988; Send et al., 1987). Hence, the estimate of *Q* here is assumed to have a 10% error.

Results

Wind Forcing

This section provides a characterization of wind forcing from three measurement sites. As data are compared from multiple locations, a standard compass coordinate system is used in this description. For the rest of the thesis, the coordinate system has positive y-axis directed along-shelf poleward and positive x-axis directed onshore.

During the summer study period, regional wind forcing over Monterey Bay as measured by NDBC buoy is similar to other west coast regions with periods of northerly upwelling-favorable winds interspersed with brief relaxation events (Figure 7). The M1 winds show a similar regional-scale upwelling/relaxation pattern but with a more prevalent diurnal-frequency component. The Long Marine Lab record (Figure 7, panel C) shows a different response during this time, namely one that is dominated by the diurnal sea breeze. The y-axis is positive westerly, showing the diurnal bursts to be oriented parallel to the inner shelf in this location (Woodson et al., 2007).

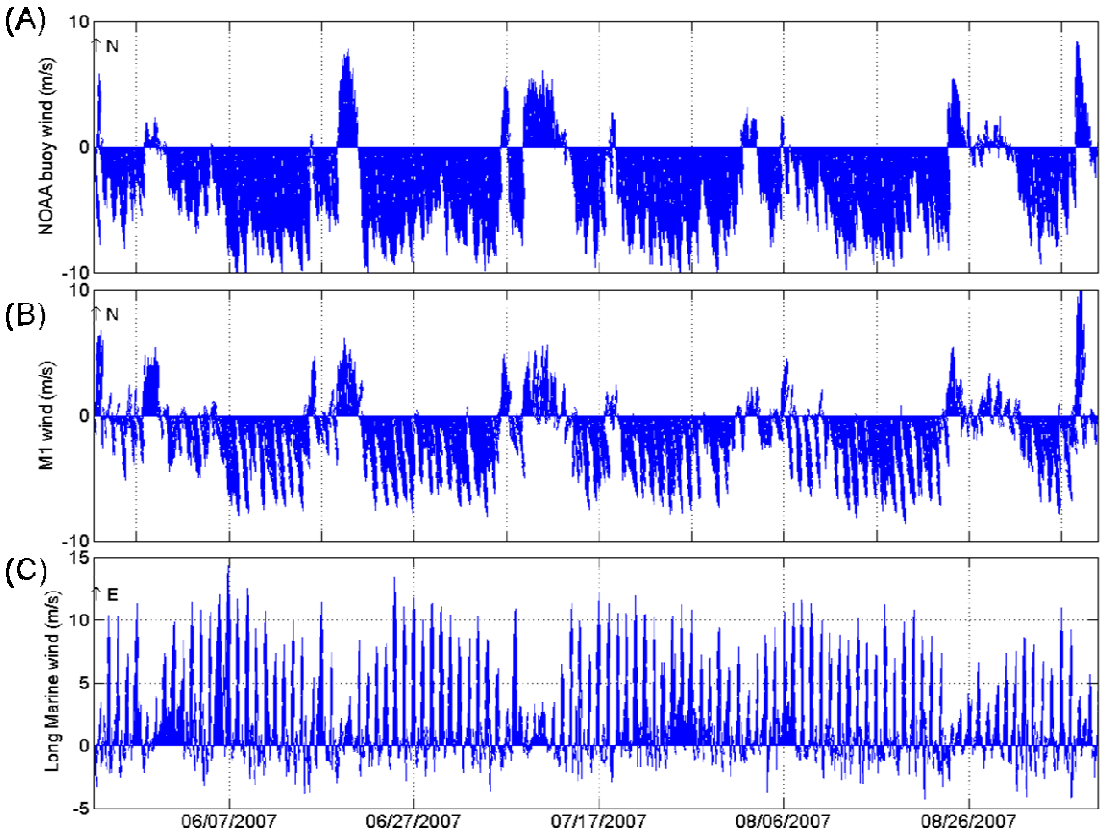

Figure 7: Vector time series from 3 wind locations in Monterey Bay. (A) NDBC buoy 46042, (B) MBARI M1, (C) UCSC Long Marine Lab. Note axis in (C) is positive westerly.

Computed power spectra of wind speed magnitude from the three locations show the power distribution as a function of frequency (Figure 8). In general, spectral shapes are similar at all three locations. Diurnal peaks due to sea breeze are evident in each spectral record (~ 0.04 cph). There is also a clear peak at the second harmonic of the sea breeze (~0.08 cph) and perhaps a hint of a peak at the third. The appearance of these higher-order harmonics in Monterey Bay wind spectra was also seen by Hendrickson and MacMahan (2009) who note that the size of the primary diurnal harmonic is 3 times the second harmonic and 10 times the size of the third (Hendrickson and MacMahan, 2009). In this work, I concentrate on the primary sea breeze harmonic centered around 0.04 cph.

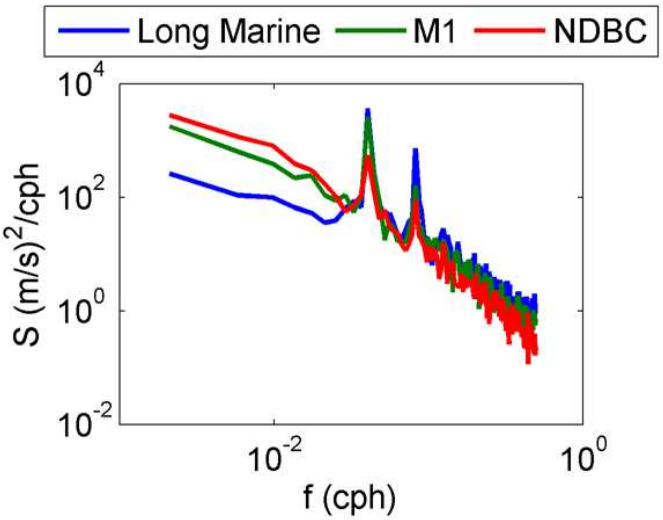

Figure 8: Power spectral density of wind speed from Long Marine Lab (blue), NDBC buoy (red), and M1 (green).

Offshore moorings (M1 and NDBC) show higher power at lower frequencies than the Long Marine record and the mean wind speed is also higher at these two offshore moorings. Diurnal band winds (defined here to have periodicity between the 18 and 33 hours) make up a portion of the variance in all three of the wind records (Table 1); the percentage is especially high at the local wind station (Long Marine).

Table 1: Wind station statistics. Percent variance in diurnal band is defined here as the percentage of wind speed variance in diurnal band (between 18 – 33 hours) divided by total wind speed variance. Ellipticity is the ratio of the length of the major axis to the minor axis. Ellipse inclination is the clockwise angle that the 1 cpd major axis makes with true north.

Location	Wind speed mean (m/s)	Wind speed stdev (m/s)	Wind speed percent variance in diurnal band	Diurnal ellipse ellipticity	Diurnal ellipse inclination
Long Marine	2.28	3.67	63%	13	261
NDBC	6.32	2.95	13%	2	293
M1	5.33	3.09	44%	3	282

Turning our attention to the diurnal band, diurnal ellipses (Table 1) calculated by least squares regression to the 1 cpd harmonic using hourly wind vectors show results consistent with previous work; the sea breeze is predominantly oriented eastward towards the Salinas Valley (e.g. Banta et al., 1993). The Ellipticity, calculated as the ratio of the major and minor axes, gives a measure of the polarization of the wind at this frequency. Diurnal Long Marine winds have largest ellipticity with winds along the major axis (oriented towards the east) an order of magnitude greater than winds along the minor axis.

Observed Currents

In this section, I present an overview of observed currents during the study period recorded by the ADCP (20-m) and AWAC (15-m) as well as similarities and differences between the two. The general description of depth-averaged and depth-dependent flows is followed by an in depth discussion of diurnal frequency motions, including the relation between currents and wind and tidal forcing.

Depth-Averaged currents

Depth-averaged flows are alongshore positive (out of Monterey Bay) (Table 2). Depth-averaged currents measured at the 20 m (ADCP) mooring are larger than those measured at 15 m depth (AWAC). Ellipticity of the principal axes shows that the depth-averaged current is predominantly alongshore with minimal flows in the cross-shelf direction, particularly at the 20 m mooring.

Table 2: Table of depth-averaged current statistics from ADCP and AWAC. Ellipticity is the ratio of the length of the major axis to the minor axis as defined by the principal axis. Angle given is the angle the major principal axis makes with true north.

Current meter	Alongshore velocity(V) (m/s) Mean	Alongshore velocity(V) (m/s) Std	Across-shelf velocity (U)(m/s) Mean	Across-shelf velocity (U)(m/s) Std	Principal axis ellipticity	Principal axis
ADCP	0.08	0.12	-0.004	0.01	126	294
AWAC	0.04	0.07	-0.003	0.01	52	278

The less ellipticity at 15 m could be indicative of 3-dimensional topographic effects as the shore is approached. There is a 16 degree difference in the angle of the two principal axes. Following the coastline from the north into Monterey Bay, Terrace Point is the location where inner-shelf bathymetry begins to diverge (see Figure 2, B). The two different angles of principal axis are consistent with a summer 2006 deployment of 2 current profilers at 20 m and 10 m depths in this location (Woodson et al., 2007). Though there are slight variations between the two measurements the alongshelf depth-averaged flows are highly correlated (CC = 0.84).

Power spectra of ADCP depth-averaged along-shelf flow shows peaks in diurnal and semidiurnal bands (Figure 9). Also noted below are four main tidal constituents and the local Coriolis frequency (0.0503 cph). There is no energetic peak at the inertial period (19.8 hours) in these spectra suggesting that the proximity to the coast damps all inertial oscillations.

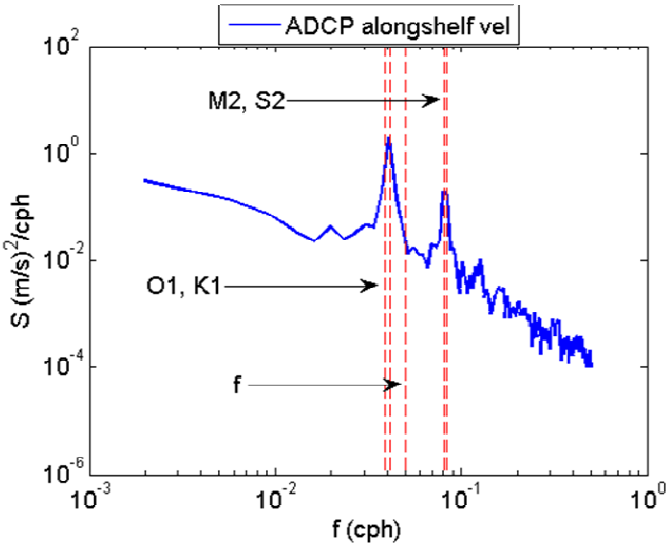

Figure 9: Power spectra of depth-averaged along-shelf current from 20-m ADCP along with red lines denoting other frequencies of interest.

Depth-dependent currents

Once depth-averaged currents are removed, we are left with depth-dependent currents in the along- and cross-shelf directions. General characteristics of these flows at different levels in the water column are presented in table 3. Currents are interpolated onto an evenly spaced grid in the vertical so water column levels are given as a percentage of the total depth (h/D) with 0% at the bottom and 100% at the

surface. At these levels, current statistics track well between the two instruments without much difference in means or standard deviations.

Table 3: General statistics of depth-dependent currents at a few depths in the water column.

Current meter	Along-shelf velocity (V) (m/s) Mean	Along-shelf velocity (V) (m/s) Std	Across-shelf velocity (U) (m/s) Mean	Across-shelf velocity (U)(m/s) Std
ADCP				
85%	0.02	0.09	-0.02	0.04
50%	0.02	0.03	0.01	0.02
10%	-0.05	0.08	0.002	0.05
AWAC				
85%	0.02	0.09	-0.01	0.04
50%	0.01	0.04	0.007	0.02
10%	-0.03	0.07	-0.003	0.04

The power spectra of depth-dependent currents show peaks in diurnal and semidiurnal bands (Figure 10). As in the depth-averaged currents, inertial energy is not significant in relation to the diurnal and semidiurnal band. Furthermore, lower frequency motions are not as energetic as the diurnal and semidiurnal frequencies.

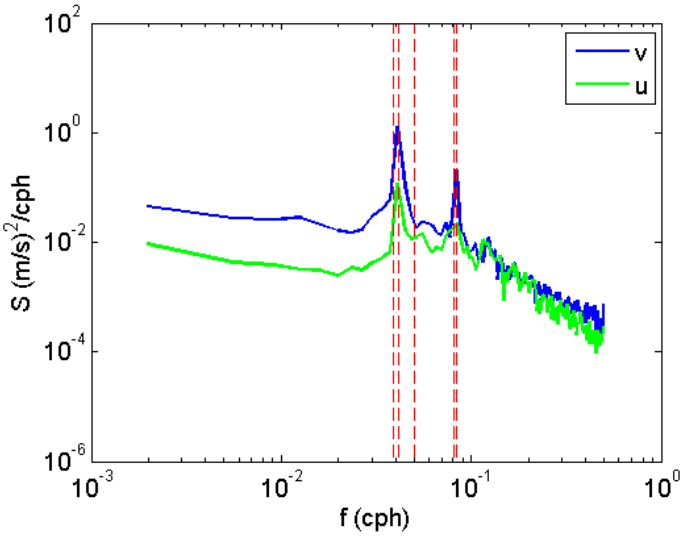

Figure 10: Power spectra plot of depth-dependent current from 20 m ADCP at 85% of water column along with 5 red lines denoting frequencies as in Figure 9 above.

Tides

One of the difficulties of working in the diurnal band is the proximity in frequency of many processes that can potentially contribute to the measured signal. The sea-breeze is a fairly narrow-banded process centered around 1 cpd, but there is possibility of signal-leakage between the sea breeze and tidal frequencies. Accurate numerical modeling of the tides throughout Monterey Bay is a current research topic, and other oceanographic studies in this location provide a resource to compare tidal amplitudes estimated here (e.g. Rosenfeld et al., 2008).

Consistent with previous results, the two largest tidal constituents identified from AWAC pressure measurements are the M2 and K1 (Rosenfeld et al., 2008) (Table 4). Though T_TIDE runs analysis on a large number of tidal constituents, only the top four constituents are needed to explain more than 90% of the variance in the pressure signal. Percent variance is defined here as the ratio of the variance in the individual sinusoid divided by the total variance of the time series.

Table 4: Top four tidal constituents from bottom pressure resolved with 30 days of data.

Constituent	Amplitude (cm)	Percent Variance Explained
M2	50	47%
K1	42	33%
O1	22	10%
S2	12	3%
	Total variance:	93%

About 45% of along-shelf velocities are described by the same top four tidal constituents (Table 5). Other constituents given through the T_TIDE harmonic analysis were smaller than 1% and not reported here. In contrast, depth-averaged velocity in the cross-shelf direction had very little percent variance explained (< 5%), and I conclude that they are not well described by the tides.

Table 5: Top four tidal constituents of depth-averaged alongshore velocity resolved with 115 days of data.

Constituent	Amplitude (cm/s)	Percent Variance Explained
M2	3.5	4%
K1	10.5	36%
O1	2.7	2%
S2	2.9	3%
	Total variance:	45%

Given that the tides are predominantly in the alongshore direction, the two tables above present an inconsistency. Bottom pressure and sea level records indicate that, like much of the West Coast, tides in Monterey Bay are predominantly semi-diurnal. However, tidal analysis on velocity records show that the larger tide (M2 - period 12.42 hours) is smaller than the K1 (period 23.93 hours) constituent by a factor

of 3. Instead of removing the diurnal tide given by harmonic analysis of depth-averaged velocity (a likely overestimate of the K1 velocity), the K1 amplitude is estimated by the ratio given in Data & Methods (Tides section), and removed from the depth-averaged velocity. Semidiurnal tides are removed from the depth-dependent velocity data with a 20-hour low-pass filter as discussed in Data & Methods.

Current/wind relation

Local wind forcing (Long Marine Lab) in this location has been identified as an important forcing mechanism of currents at seasonal scales (Drake et al., 2005). Cross-shelf currents are also coherent with water column temperature fluctuations, helping to determine the existence of diurnal upwelling (Woodson et al., 2007). Here I further examine the relation of the local wind to diurnal-period currents. Winds are rotated so that their axis is aligned with the isobaths as defined by the principal axis of the depth-averaged current at the two different current meters giving alongshore and across-shelf wind components at each location.

There is some ambiguity in interpreting correlation values between currents and wind forcing separated into along- and across-isobath components because the along and across-isobath winds are themselves anti-correlated (CC = -0.66) at the same level as the correlation with currents (Table 6). However, correlations between depth-averaged along-shelf currents and both wind components are significantly higher than correlations between the depth-averaged cross-shelf currents with the wind.

Table 6: Correlation coefficients between wind components and depth-averaged current components. (*) Correlations not significant at 95%

Current meter	Correlation of *V* to *v-wind*	Correlation of *V* to *u-wind*	Correlation of *U* to *v-wind*	Correlation of *U* to *u-wind*
ADCP	0.66	-0.66	0.06*	0.07*
AWAC	0.63	-0.58	-0.29*	0.2*

In the upper water column, along-shelf currents still correlate well with the wind (Table 7). In addition, there are significant correlations between depth-dependent cross-shelf currents and along-shelf winds. There are also significant anti-correlations between cross-shelf motions in the upper water column and cross-shelf winds. Other inner-shelf studies have found cross-shelf motions effectively driven directly by cross-shelf wind forcing (e.g. Fewings et al., 2008; Tillburg, 2003). In these studies the correlation between cross-shelf currents in the upper water column and cross-shelf winds is positive. As the cross-shelf wind is not directly driving cross-shelf currents in this location, I consider dynamics involved in cross-shelf motions driven by cross-shelf wind unimportant and instead examine processes that explain cross-shelf motions driven by along-shelf winds.

Table 7: Correlation coefficients between 20-hr low-passed wind and depth-dependent current components at 85% of the water column.

Current meter	Correlation of *v* to *v-wind*	Correlation of *v* to *u-wind*	Correlation of *u* to *v-wind*	Correlation of *u* to *u-wind*
ADCP 85%	0.83	-0.83	0.7	-0.43
AWAC 85%	0.66	-0.61	0.57	-0.52

Ekman Transport Percentages

At subtidal frequencies, previous studies have found that 100% of Ekman transport is realized at around 50 m water depth and decreases to 25% in 15 m (Lentz et al., 2001; Kirincich et al., 2005). The diurnal wind forcing at Terrace Point is strong and predominantly along-shelf, thus we might expect that a percentage of offshore Ekman transport will also be realized, delivering cold subsurface water to the inner shelf at this location (Woodson et al., 2007). Furthermore, diurnal ellipses calculated

from ADCP velocities in the upper water column (70% - 85% of water depth) were oriented to the right of the wind ellipse by $49^{o} \pm 2^{o}$, consistent with Ekman theory (Ekman, 1905). As described in Data & Methods (Ekman transport section), the fraction of Ekman transport realized at the two depths attributable to diurnal period winds is estimated through neutral regression. Depth-dependent currents are integrated from the first zero crossing to the surface. Extrapolation of measured currents from the shallowest good bin to the surface is needed to get an accurate magnitude of transport from the zero crossing and results are compared from both slab and linear extrapolation (Table 8).

Table 8: Comparison of correlations and fractions of ekman transport realized for at both instruments.

Current meter	Correlation of measured to theoretical transport	Fraction of realized transport (slope of linear regression)	Intercept of linear regression
ADCP			
linear	0.65	0.80 ± 0.12	-0.006 ± 0.03
slab	0.64	0.77 ± 0.12	-0.008 ± 0.03
AWAC			
linear	0.78	0.38 ± 0.10	0.02 ± 0.02
slab	0.77	0.36 ± 0.09	0.02 ± 0.02

Transport percentages are not significantly affected by the extrapolation technique used. Following Kirincich et al. (2005), there are two criteria fulfilled by both significant results. The first is that depth-averaged cross-shelf current does not correlate with wind stress (Table 6), consistent with the assumption of 2-dimensional dynamics. The second criteria is a high correlation between theoretical and measured transports (Table 8). Also following Kirincich et al. (2005), the intercept from neutral regression should not be significantly different from zero. This would indicate surface

transports forced by factors other than the along-shelf wind stress, not included in the regression model. Intercepts are very close to zero for the ADCP and slightly further from zero at the AWAC.

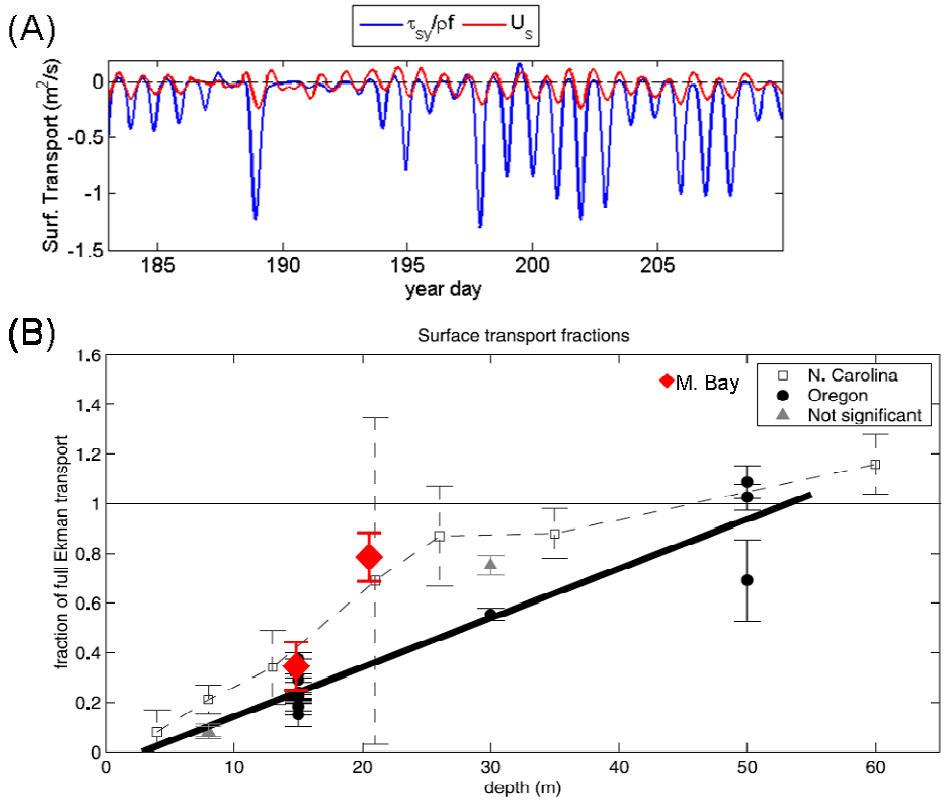

Figure 11: (A) A subset of the time series comparing theoretical and measured surface transport. (B) Fraction of full Ekman transport at a variety of inner shelf locations. Figure reproduced from Kirincich et al. (2005). Added to the plot are the two (red diamond) estimates of percent Ekman transport with 20-hr low pass filtered data from this study.

If Ekman dynamics explain offshore surface motions due to along-shelf forcing, a feature that is unexplained by these dynamics is the measured onshore motions (Figure 11, panel A). These are not forced by along-shelf winds as the wind stress in this direction hardly crosses zero. They are also not forced by the cross-shelf winds as these motions are in anti-phase with the onshore wind. Woodson et al. (2007)

speculate that the onshore motions result from an unbalanced pressure gradient. Though we are still attempting to substantiate this dynamically, the effect of these motions can be seen in the heat budget results below.

Stokes' Drift

Recently, several studies have begun to document the effect of surface gravity waves on cross-shelf circulation on the inner-shelf (e.g. Lentz et al., 2008; Kirincich et al., 2008; Hendrickson and MacMahan, 2009). Following these works, I search for evidence of subtidal wave-driven circulation in this inner shelf location.

The motivation and method of transforming offshore, NDBC measured waves at this location is given in Data & Methods. The theoretical Eulerian return flow calculated from transformed buoy observations is small (Figure 12). They amount to depth averaged cross-shelf flows (mean = 0.3 cm/s, stdev = 0.2 cm/s), an order of magnitude smaller than wind-driven velocities, but comparable to observed depth-averaged cross-shelf velocities.

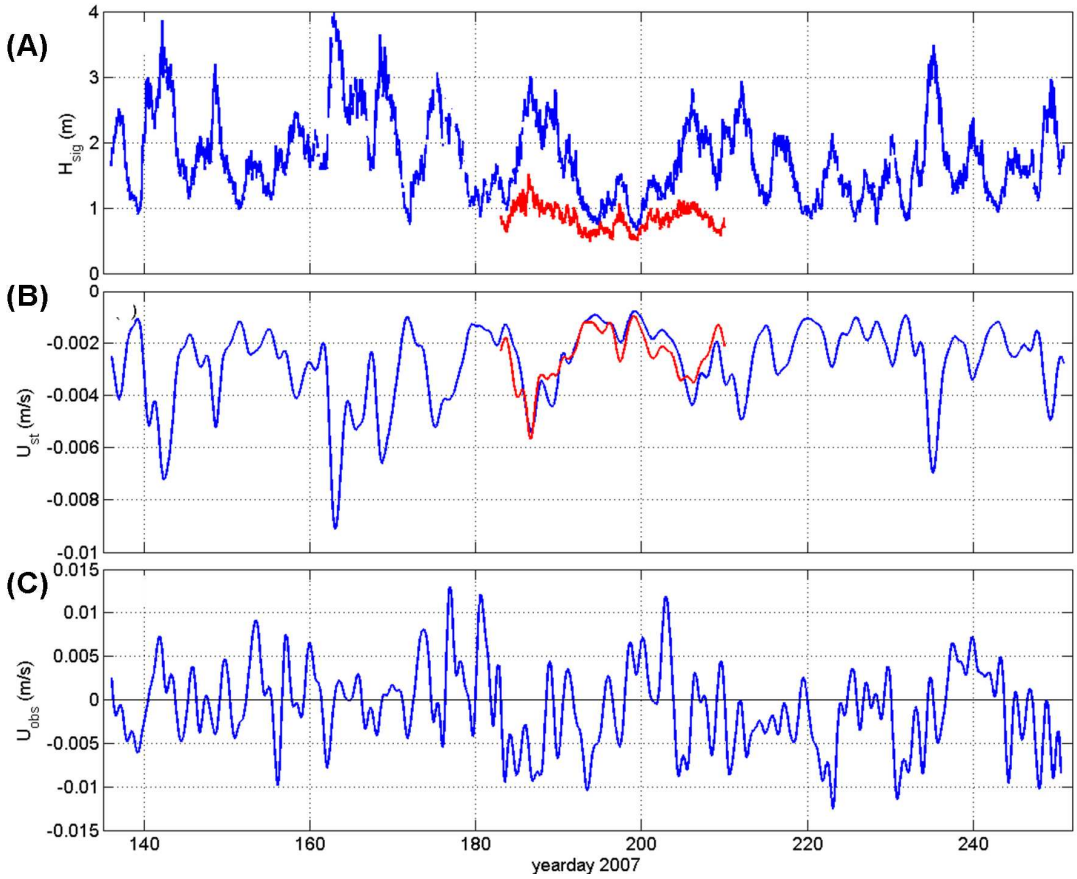

Figure 12: (A) Significant wave height at offshore NDBC buoy (blue) and measured by AWAC (red). (B) Theoretical depth-averaged Stokes' velocity using AWAC measured waves (red) and buoy transformed wave heights (blue). (C) Measured depth-averaged cross-shelf velocity from ADCP.

However, the correlation between the observed cross-shelf depth-averaged velocity from ADCP and the Stokes' velocity was insignificant (CC < 0.05). For comparison, the lowest correlation from an Oregon study was 0.21 (Kirincich et al., 2008). In their study, Kirincich et al.(2008) found that the correlation changed slightly with different extrapolation techniques and rotations, but not significantly. They also defined their principal axis by subtidal depth-averaged velocities during periods of low wave forcing (Hsig < 1). At our location, significant waves rarely reached 1.5 m and rotating depth-averaged currents by a few degrees did not substantially change correlation values.

Another way of viewing the relationship between observed and theoretical depth-averaged return flow is by binning observations into Hsig/h bins. As we occupy a smaller parameter space than previous studies due to small observed waves, no significant trend can be discerned here either (Figure 13).

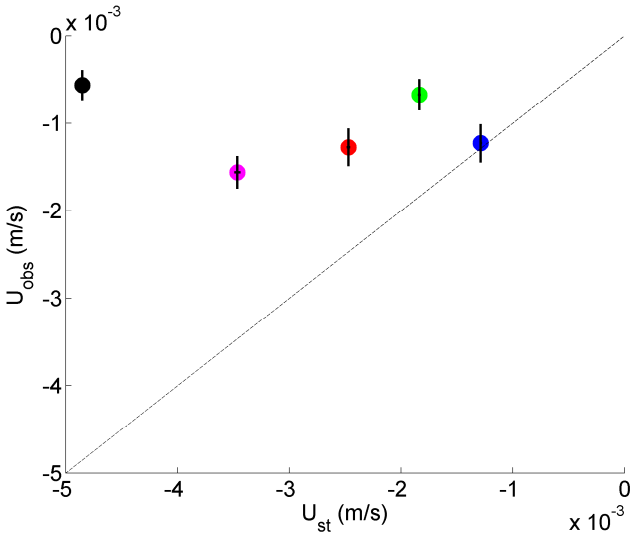

Figure 13: Depth-averaged theoretical return flow Ust versus observed depth-averaged cross-shore flow (Uobs) where observations are placed in Hsig/h bins going from smallest ratio (blue = 0.058) to highest (black = 0.16).

The insignificant correlation between the time series of observed depth-averaged cross-shelf velocity and theoretical Stokes' return along with the weak relationship in the scatter plot above points to the lack of surface gravity wave influence on the cross-shelf circulation in the inner shelf at this location.

Temperature and Heat Balance

Presented here is an overview of temperature measurements from TPT 20-m thermistors (map in Figure 2). Also discussed are the relationship of these measurements to wind and tidal forcing as well as the first part of analysis on the heat

balance for this location. The focus is on the 20-m thermistor chain as there was a long-term ADCP deployed at this position and it was in the middle of the cross-shelf array.

Terrace Point Temperatures

On average, temperatures during the study period showed a stable water column with warmer temperatures at the surface, and decreasing with depth (Table 9). Temperature variations were larger towards the surface as evidenced by lowest measured standard deviations at the bottom thermistor.

Table 9: Temperature statistics for Terrace Point 20m array.

TPT Thermistor	Mean (oC)	Std (oC)
0 m	14.3	1.37
5 m	13.1	1.36
10 m	12.1	1.29
19 m	10.7	.82

More so than local winds or currents, temperature spectra show energetic low-frequency modulations (Figure 14). These will not be discussed here but are most likely associated with large-scale processes that affect the entire Monterey Bay (e.g. Rosenfeld et al., 1994; Ramp et al., 2005). Here I focus on the daily modulation of temperature at this location.

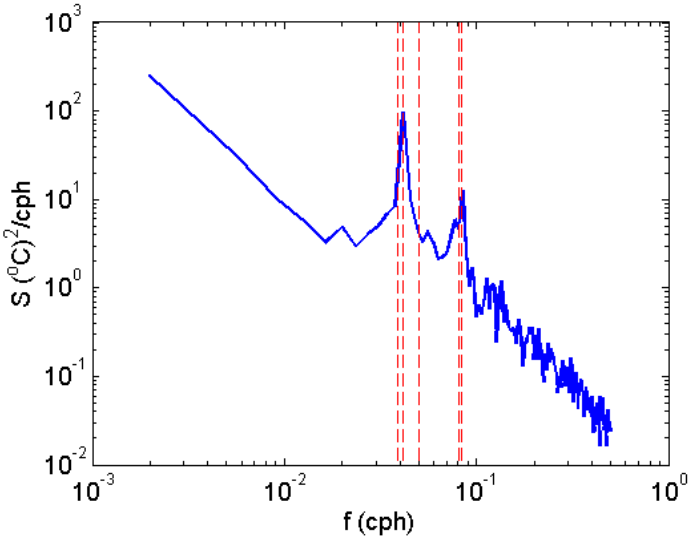

Figure 14: Power spectra plot of temperature from 20-m TPT mooring at 5-m depth with 5 red lines denoting frequencies as in Figure 9.

As with currents, temperature power spectra show large peaks at the diurnal and semi-diurnal frequencies close to known tidal frequencies. Results from tidal analysis with T_TIDE are shown for the top four tidal constituents (Table 10), the sum of which explains 40% of the temperature variance.

Table 10: Top four tidal constituents of temperature resolved with 80 days of data.

Constituent	Amplitude (oC)	Percent Variance Explained
M2	0.09	3%
K1	0.66	25%
O1	0.06	2%
S2	0.27	10%
	Total variance explained:	40%

Semidiurnal tides should be dominant in this region and the larger contribution of the K1 compared to M2 is indicative of other processes at the diurnal frequency being responsible for temperature modulation. The correlation between temperature and sea breeze winds was maximum at 5 m (0.53) with a lag of 7 hours. These results are consistent with a previous study (Woodson et al., 2007).

Heat balance at Terrace Point

Daily incoming solar radiation peaks between 10 am and 3 pm. However, increases in measured temperature do not coincide with this period and instead temperatures warm in the evening and overnight (Figure 15) (Woodson et al., 2007). The counterintuitive timing of warming periods point to the need to understand the heat balance at Terrace Point. Here I compare finite difference estimates from in situ data of the various terms in the following heat equation, as described in the methods section.

$$\frac{\partial H}{\partial t} = Q - u\frac{\partial H}{\partial x} - v\frac{\partial H}{\partial y}$$

To estimate the relative contributions of the three terms on the right hand side, each term is integrated during times of increasing heat content (Figure 15, panel B).

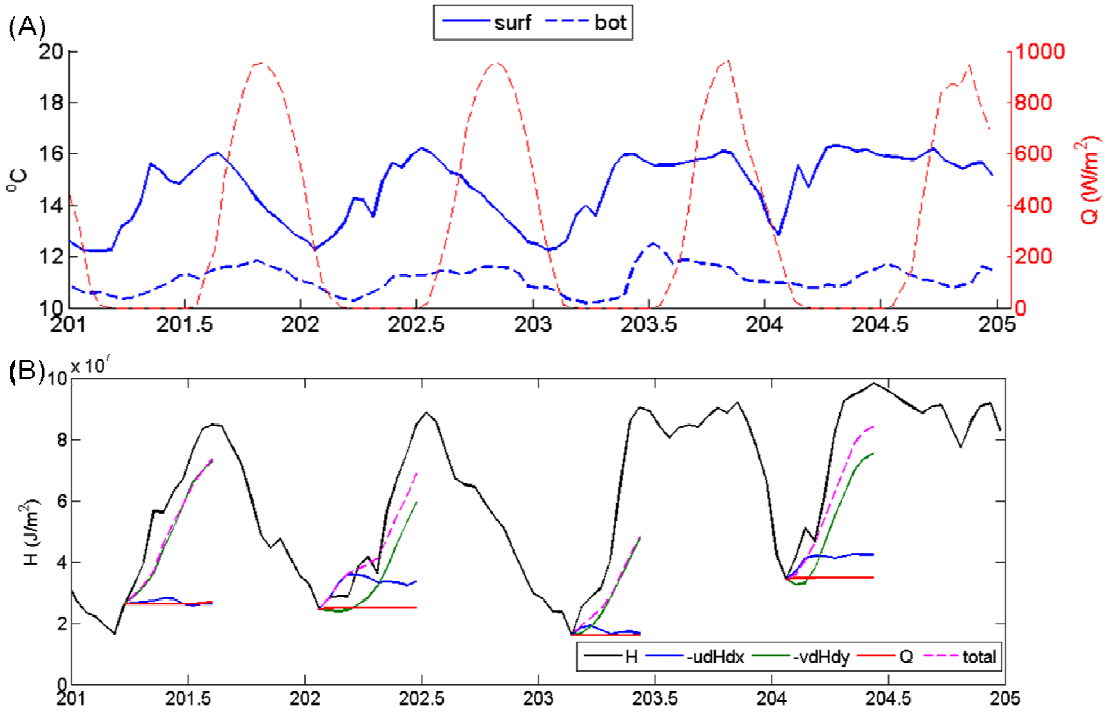

Figure 15: (A) Temperature time series at TPT 20-m from surface (solid) and bottom (dotted). Also shown is incoming solar radiation (dotted red). (B) Time series of estimated heat content (H), time integral ($\int dt$) of 3 terms on the right hand side of heat equation and the sum of these (dotted magenta).

As in Send et al. (1987), the slope of a linear regression comparing each term to the total observed change in heat content ($\int \partial H / \partial t$) gives an approximate percentage of how much heating is due to each individual term (Table 11).

Table 11: Slope of linear regression giving percentage of variance in observed heat increase for each day.

Heating term	Day 201	Day 202	Day 203	Day 204
Q	0.4%	0.3%	0.0%	0.4%
Cross-shelf advection	-1%	4%	-1.5%	9%
Along-shelf advection	91%	53%	41%	70%

These initial results show that along-shelf advection of the thermal gradient between Sand-Hill Bluff and Light House Point is responsible for most of the observed warming, with little warming due to cross-shelf advection and an even a smaller percentage due to solar heating. This calculation uses hourly data and only 6 points during each warming period are used in the regression. A more complete treatment will be given in the "Canonical day" section including a similar analysis for the cooling periods.

Canonical Day

This section presents the results of ensemble-averaging days with strong westerly sea breeze (maximum winds reaching at least 8 m/s). This is first used as a descriptive and summarizing tool to show the average cycling of wind, currents, and temperatures. It is then used in a quantitative manner to show the daily co-variation of stratification and currents (Richardson number), and to revisit the heat balance calculation above.

General description

A summary of wind, currents, and the TPT cross-shelf temperature structure (< 20-m depth) for a subset of hours in the average day are shown in figure 16. Westerly wind begins to blow in the late morning, and undergoes an approximately 8-hour period of increasing intensity until peaking around 2 pm local time (Figure 16, panel A). Winds then die down in a similar fashion and remain calm overnight. The variation of currents with depth (panel B) shows the along- and across-shelf current response to this wind. Along-shelf (red) currents begin the day flowing out of the bay (towards positive y-axis). As the wind builds, surface currents are reversed and are directed into the bay. Eventually flow throughout the water column is directed

downwind. In the cross-shelf direction (blue), currents begin with fairly little vertical structure. As the wind builds, surface currents are directed offshore (towards negative x-axis) with opposing flow at depth.

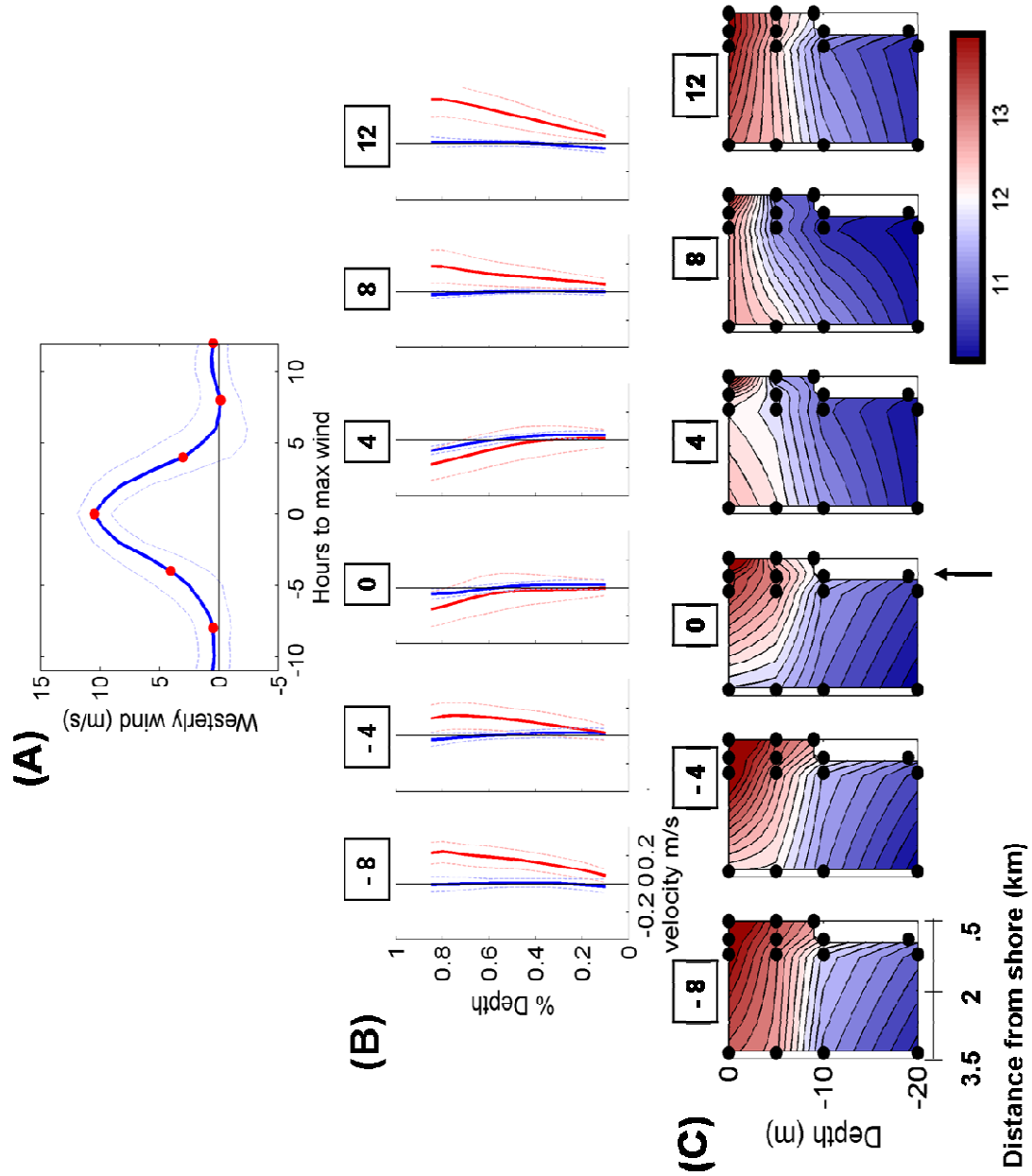
(A)
Westerly wind (m/s)
15
10
5
0
-5
-10
-5
0
5
10
Hours to max wind
(B)
% Depth
1
0.8
0.6
0.4
0.2
0
-8
-4
0
4
8
12
(C)
velocity m/s
-0.2
0
0.2
Depth (m)
0
-10
-20
3.5
2
.5
Distance from shore (km)
11
12
13

Figure 16.

Figure 16: (A) Average westerly winds. Six red dots are the hours shown in panels of (B) and (C). (B) average current profiles showing along-shelf (red) and cross-shelf currents (blue). Along-shelf currents are positive flowing out of Monterey Bay, cross-shelf currents are positive onshore. (C) Contour plots of temperature from TPT cross-shelf array. Arrow denotes location of 20-m thermistor chains. All plots show the 45-day mean for the hour. In (A) and (B) thin dotted lines denote standard error.

Temperature sections show relatively warm water overlying cool (panel C). As the wind builds, temperature drops throughout the water column at the 20-m thermistor chain (denoted by black arrows, 1 km from shore). As winds relax, surface temperatures rewarm.

Richardson Number

Hourly Richardson number estimates were made at three levels in the water column. The percentage of these that fell below the critical value for shear mixing (<0.25) is shown in figure 17 below.

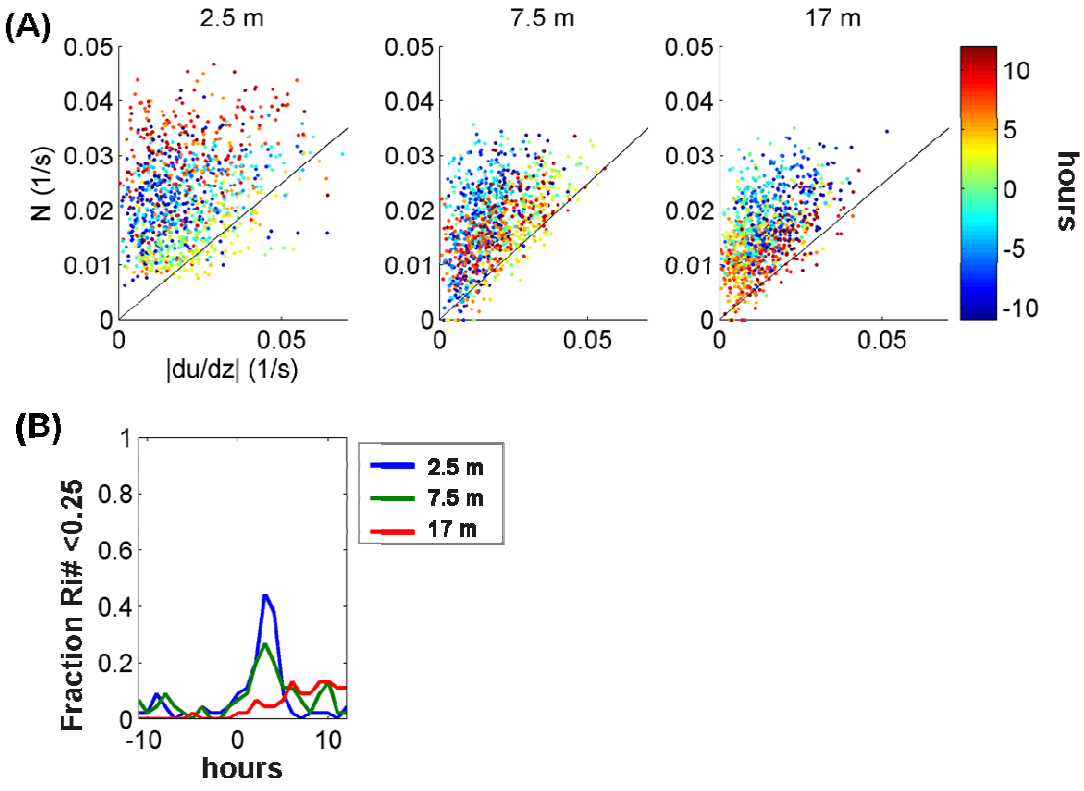

Figure 17.

Figure 17: (A) Scatter plot of |du/dz| versus N for all hours used to construct canonical day. Black line has a slope of 0.05, points below which correspond to values below a critical Richardson number of 0.25, color denotes hour leading up to and following maximum wind. (B) Average day hour versus fraction of Richardson number < 0.25 for each hour at 2.5-m (blue), 7.5-m (green), and 17-m (red) water depth.

Near-surface and mid-water column Richardson numbers show a dramatic increase in this percentage near the peak westerly wind. In fact, between 20 - 40% of the hourly Richardson numbers are below critical. This suggests that wind-induced current velocity shear is strong enough to overcome the upwelling shadow stratification and potentially mix both near-surface and mid-water column properties.

Heat budget

As in the previous heat balance discussion, various terms in the heat equation can be estimated with canonical day values of temperature, velocity, and incoming solar radiation. Panel (A) in figure 18 shows the average daily cycle of heat content at the TPT 20-m mooring along with a 1 cpd harmonic fit. The canonical day is a combination of a cooling period in the afternoon along with an evening and early morning warming period. Panel (B) shows the daily variations in three terms of the conservation equation. Incoming solar radiation is a positive contribution (warming) and peaks a few hours before maximum wind. The cross-shelf advection term is also primarily positive, while along-shelf advection shows morning and evening warming with a shorter period of midday cooling.

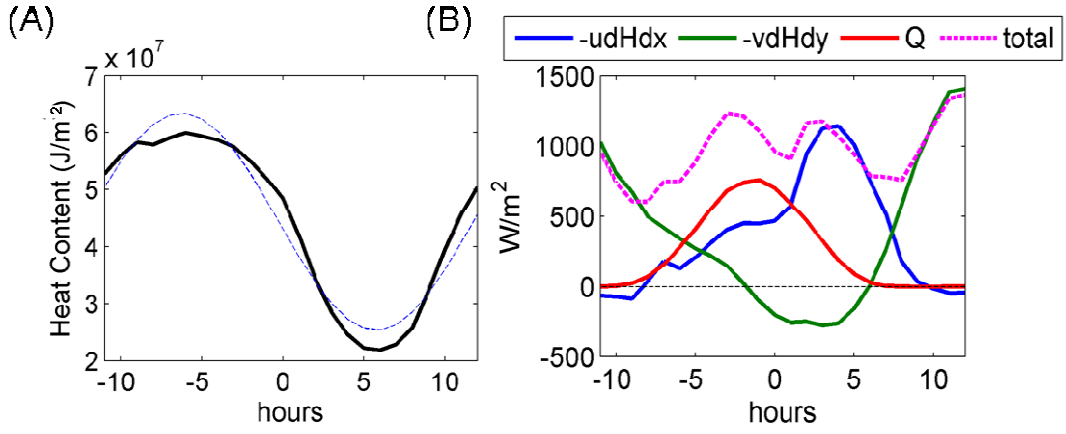

Figure 18.

Figure 18: (A) Average change in heat content for a 5-m thick surface layer at TPT 20-m (thick black line). Thin dotted blue line is 1 cpd fit. (B) Hourly canonical day values of different terms in the heat equation. Also included is the sum of the three terms (magenta).

The near-sinusoidal form of the observed daily heat content allows for creation of a longer time series by repeating the cycle. This has the advantage of combining the early morning and evening heating periods. As previously, the three heat equation terms that can be directly estimated from the data are integrated during the warming period (figure 19, panel A) and compared with the total change in heat content. Previously, linear regression was used to compare each term with the observed heating. In addition, an hour by hour fraction of each term to the observed total heat change is also shown (figure 19, panel B). While the slopes from linear regression (table 12) give a single percentage explained by each term, the hourly fraction also provides time-dependent estimates.

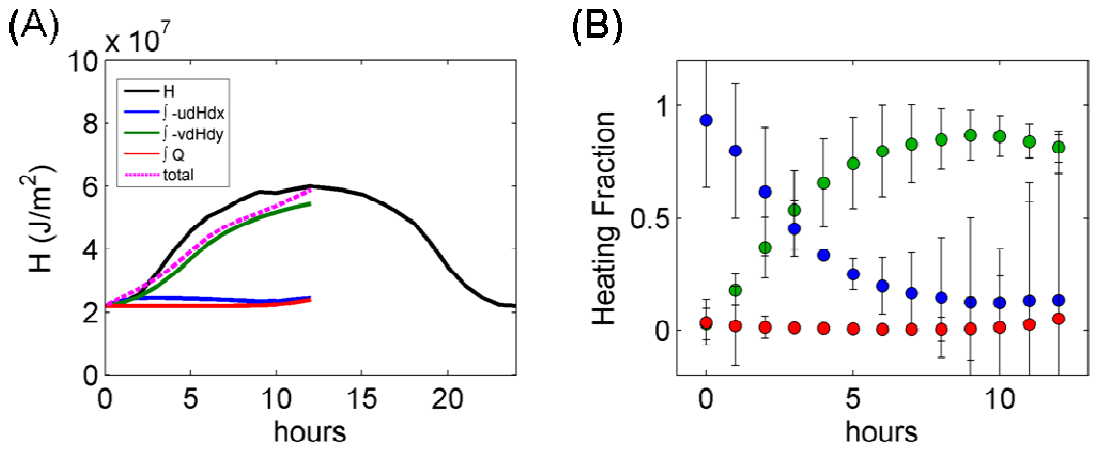

Figure 19: (A) A 24 hour time series of heat content (*H*) with integrated heat balance terms during the heating period. Note: t = 0 hours corresponds to 6 hours after maximum wind in figure 18. Total (magenta) is the sum of the three estimated terms. (B) Hourly fraction of integrated term to total observed heating.

Table 12: Slopes of linear regression give percentage of observed heating and cooling explained by each directly observed term along with 95% confidence levels. (*) The total explained cooling is less than 0%.

Heating term	Warming	Cooling
Q	2% ± 2%	-47% ± 6%
Cross-shelf advection	2% ± 2%	-60% ± 9%
Along-shelf advection	92% ± 13%	11% ± 3%
Total explained:	95% ± 14%	*

From linear regression, about 95% of the warming period can be explained by these three terms with along-shelf advection of the temperature gradient between SHB and LHP contributing over 90% of the warming. Time-dependent fractions (figure 19, panel B) also show that the along-shelf advection contributes the largest fraction of the observed heating.

Turning attention towards the cooling period, the only directly estimated heat balance term which represented a decrease in heat was along-shelf advection (figure 18, panel B). However, this term only contributes about 10% of the observed cooling (table 12). In conjunction with both Q and cross-shelf advection acting as sources of heat, the vast majority of cooling is unexplained by these terms directly estimated from data. This unexplained cooling can be accounted for by including a term not needed to close the heat balance during warming periods; vertical advection of the temperature at 5-m depth ($w_{(-5)}\rho Cp(T_{(-5)} - T_{ref})$).

As shown in Data & Methods, with an estimate of horizontal distance over which upwelling is occurring and a measured offshore mass flux, the continuity equation in 2 dimensions allows for determination of vertical velocity (w). Using measured canonical day offshore mass flux and adjusting the horizontal distance over which upwelling is occurring, vertical velocities are estimated such that the addition of the vertical advective term closes the heat balance to within 5% as defined by linear regression (closure that is comparable to warming periods) (figure 20).

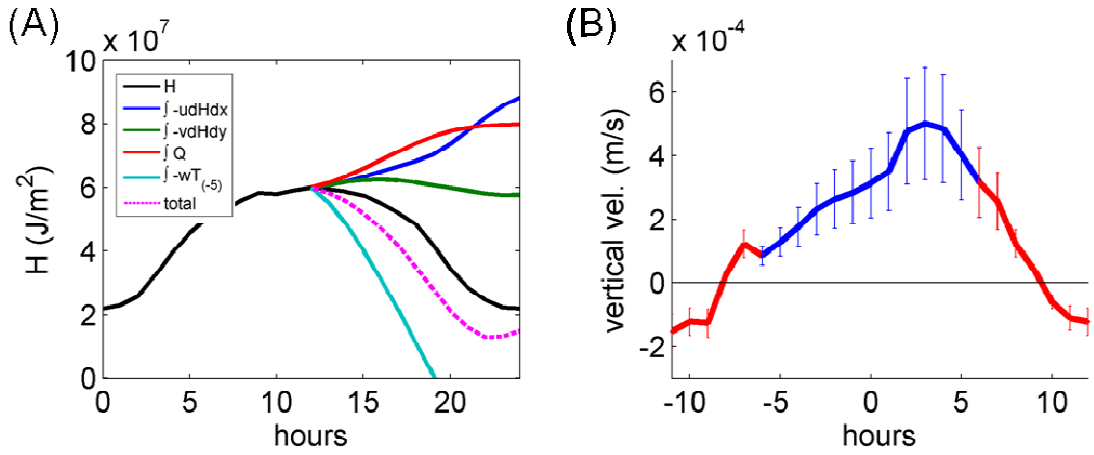

Figure 20: (A) 24 hour time series of heat content (*H*) with integrated heat balance terms during the cooling period including the estimated vertical advection. Total (magenta dashed) is the sum of the four terms. (B) Vertical velocity estimated from 2-dimensional continuity assumption. Cooling (heating) periods are marked in blue (red).

The conservation equation now written with the vertical advective term:

$$\frac{\partial H}{\partial t} = Q - u\frac{\partial H}{\partial x} - v\frac{\partial H}{\partial y} - w_{(-5)}\rho Cp(T_{(-5)} - T_{ref})$$

closes the heat balance for the cooling period in the canonical day. The total cooling (magenta dashed line figure 20, panel A) includes the cooling contribution of vertical upwelling velocity (figure 20, panel B) over a 800 m ± 75 m wide horizontal swath extending from the 20-m TPT mooring towards the coast. This estimated distance of active upwelling is less than the total distance between the 20-m mooring and the coast (1 km), the baroclinic Rossby radius (3 km), and is much less than the width of the shelf (distance from shore to 200 m isobath is approximately 16 km).

Estimates of a mean upwelling velocity are also made by examining the vertical displacement in time of the canonical day isopycnal field. The slopes of 2

isopycnals (1025, 1025.2 kg m^{-3}) are estimated from all 3 moorings on the TPT cross-shelf array (10, 20, 30 m depths) and are comparable with the continuity estimate of upwelling velocity from above (Figure 20).

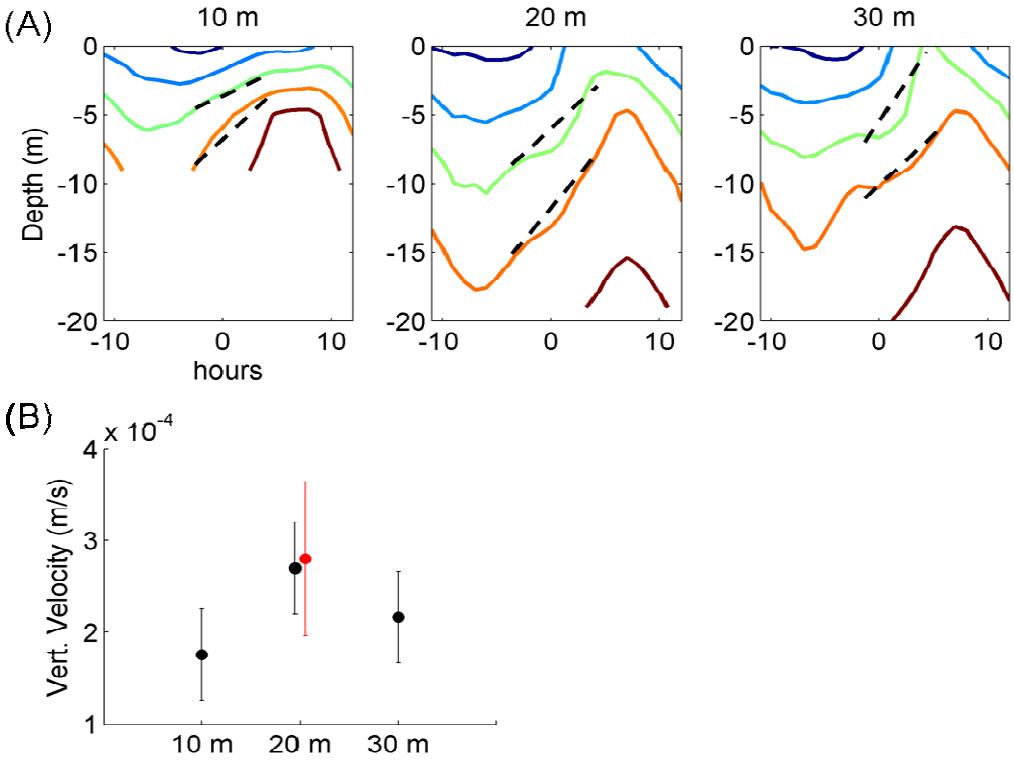

Figure 21: (A) Time vs. depth isopycnal contours with the slopes of 2 isopycnals (1025 (green) and 1025.2 (orange)) given as dashed black lines from the three cross-shelf moorings. (B) Estimates of mean upwelling from isopycnal displacements (black), and mean upwelling velocity from 2-dimensional continuity (red).

Discussion

Wind Forcing

Previous work has shown measured currents at this location to correlate better with local winds than regional ones (Drake et al., 2005). Thus, in this thesis I have focused on local wind forcing. Here, 63% of wind speed variability is in the diurnal band. These sea breeze winds are strongly oriented in the along-shelf direction. This is an unusual forcing which contrasts with other coastal sea breeze studies where winds blow across the shore in accordance with a standard land/sea breeze circulation (e.g. Rippeth et al., 2002). Due to slight differences between topographic shoreline and bathymetric orientation, there is a small component of the diurnal winds that blow across shore as well. While other studies find cross-shelf currents driven by cross-shelf wind forcing (e.g. Fewings et al., 2008; Tillburg, 2003), the correlation found here is negative (CC = -0.43) and cross-shelf winds are not an effective mechanism of directly driving cross-shelf currents.

Tides

In this study, harmonic tidal analysis estimated depth-averaged diurnal tidal velocities larger than semidiurnal ones. This is in contrast to the fact that West Coast tides are predominantly semi-diurnal, suggesting that diurnal tide and sea breeze signals are indistinguishable in our record. The Rayleigh criteria gives an estimate of the length of a data record needed to separate between two sinusoidal signals. According to this criteria, the record length required to differentiate between the K1 (23.93 hours) tidal constituent and a 1 cpd (24 hours) harmonic is 342 days. Other authors have found that even with such a long time series at this location, the depth-averaged K1 tidal constituent is still larger than the M2 (Rosenfeld et al., 2008). In another study (Cadiz Bay, Spain, 36.5o N), observations and modeling efforts have

also showed a seasonal variation in the K1 tidal constituent as it responds modulation by the strength of the sea breeze (Alvarez et al., 2003). These authors conclude that this reflects the depth-averaged tidal velocity is corrupted by the sea breeze. Further complicating matters, the sea breeze signal is nonstationary and smears into a band of frequencies rendering it inseparable from close tidal frequencies regardless of record length.

The method used here of accounting for diurnal tidal currents by forming a ratio between bottom pressure estimates at tidal frequencies to predict the ratio of tidal velocities at these same frequencies is also imperfect and leaves ambiguity in what the actual tidal velocities are. It does however give an upper bound to the amount of the velocity signal attributable to the tide. The canonical day showed along-shelf flow initially directed out of Monterey Bay. As winds intensify, currents at all levels in the water column reverse and are directed in the along-wind direction (into Monterey Bay). Though these hourly velocity profiles might still contain diurnal tidal effects, the tidal ratio shows that tides would not account for more than 0.03 m/s of what is seen in the profiles.

Though not a focus of this thesis, there is also significant energy at the semidiurnal frequency in both depth-averaged and depth-dependent velocities. A previous study has shown that along the inner shelf near this location (3km north), semidiurnal tidal energy can break into packets of internal waves that propagate onshore (Storlazzi et al., 2003). Effects of the semidiurnal and surface and internal tides were removed in our calculations in two ways. For Ekman transport calculations we use low-pass filtered (20-hr cutoff) velocities. For the canonical day, 45 different days spanning nearly 2.5 months were averaged together, blurring the phase of semidiurnal tides.

Waves

With summertime waves in the region dominated by northern swell and perhaps due to coastline orientation, the location of Terrace Point appears to shield it from much of the regional wave forcing and this work shows wave-driven flows to be unimportant on this inner-shelf. In contrast, recent work from across Monterey Bay (Marina, CA) has shown the importance of sea breeze in modulating significant wave heights, substantially affecting inner-shelf current profiles year-round (Hendrickson and MacMahan, 2009). Other wave-forced inner-shelf studies had long records, multiple instrument locations, and a variety of seasonal conditions that allowed for separation between wind-driven and wave-driven periods. During the study period in our location, there was not much variation in wave heights and wind forcing was almost always present. Perhaps a more detailed study would find different results.

Ekman Transport Percentages

One of the questions we hoped to answer was what fraction of Ekman transport is realized at near-inertial timescales? In this work, the percentage of realized theoretical surface Ekman transport is within the error of percentages found for the same depths (15 – 20 m) in previous studies (Lentz, 2001; Kirincich et al., 2005), though the error bars for the 20 m site appears abnormally large, perhaps due to lack of data (Figure 11). These studies focused on the inner-shelf response to low frequency (periods > 40 hour) along-shelf winds. Ekman's original theory assumes a steady balance between the Coriolis force and turbulent stress divergence. A scaling of the time-dependent Ekman balance gives the amount of time to reach steady state to be one inertial period divided by π (for this latitude $T_i/\pi \sim 6$ hours). The results here suggest one of two things. Either the spin up of the surface Ekman layer occurs within the time of sea breeze wind forcing (~ 10 hours) and steady Ekman dynamics are a good approximation, or it is more appropriate to compare offshore transports driven by periodic forced oscillations to a different quantity than given by steady Ekman

dynamics (τ /ρf). A simple 1.5 layered model driven by oscillatory surface forcing is derived in Cushman-Roisin (1994) and shows the potential for a large resonant flow response to near-inertial forcing, perhaps explaining the high percentage of theoretical Ekman transport realized in northern Monterey Bay. The applicability of this theory to the inner shelf will require further observational studies and modeling efforts.

Correlation between surface transport and along-shelf winds was an important criteria for Kirincich et al. (2005) to accurately interpret their transport fractions as due to along-shelf winds. In our study, prior to calculating the regression, we lagged the two time series (measured transport and theoretical transport) to the hour of maximum correlation (transport lags wind by 3 hours). Application of a lag as described here was not seen in the methods of the prior studies perhaps due to this lag being small in comparison to the highest resolved frequency of their time series (periods >40 hours).

Though not reported in detail, bottom transports were also calculated as a further check of 2-dimensional dynamics. For most of both ADCP and AWAC records, there was only one zero crossing near the middle of the water column resulting in a simple 2-layer flow with equal and opposite transports between the two layers.

Canonical Day Heat Budget

The shadow zone in the northern part of Monterey Bay is characterized by water that is warmer than waters within the offshore upwelling jet (e.g. Rosenfeld et al., 1994). The shadow and upwelling jet are separated by a sharp front and recent work with this 2007 PISCO data set shows that the cross-shelf array at TPT was consistently within the upwelling shadow during the study period, while the array at SHB experienced frequent frontal crossings (Woodson et al., 2009). Our results show that daily warming events at TPT are caused by along-shelf advection of the gradients within the shadow and not advection of the upwelling shadow front past TPT.

Previous work on the development of the upwelling shadow has stressed the particular susceptibility of this location to solar radiation and the trapping of heat in the upper water column (e.g. Graham and Largier, 1997). Estimates of heating due to solar insolation in the shadow have varied from 0.5 degrees/day (Graham and Largier, 1997) to 2 degrees/day (Ramp et al., 2005). The location of TPT is close to the western edge of the shadow where the effects of solar heating are in competition with diurnal upwelling that cools the water column (Woodson et al., 2007).

While the canonical day showed the heat balance was satisfied for the warming period by three terms estimated directly from data, cooling periods were not. Cooling happens during midday at times of along-shelf westerly sea breeze forcing. Consistent with along-shelf uniformity, offshore surface motions resulted in vertical advection of cold water from below that closed the heat balance to within 5%. The upwelling velocities estimated by 2 independent methods were comparable to previous findings (Woodson et al., 2007). The region of active upwelling extended over a 800 m ± 75 m wide cross-shelf horizontal swath, a number smaller than both the shelf width (16 km) and the baroclinic Rossby radius (2 km). If upwelling is assumed to occur within the Rossby radius, these vertical velocities would be even smaller and thus not capable of accounting for the observed cooling. Previous work on the inner-shelf divergence of Ekman transport has showed a linear decrease in the percentage of realized transport from 50-m depth to the coast (Lentz, 2001; Kirincich et al., 2005). This also suggests a linear decrease in upwelling intensity as the coast is approached. A comparison of upwelling velocities estimated from moorings at three inner-shelf depths in this study did not discern a significant difference between the three. Further measurements are needed to accurately distribute upwelling velocities over a larger swath.

The addition of the vertical advection term to the heat equation during cooling periods gives rise to the question of whether or not this term also affects the balance during the heating periods. The estimated vertical velocity did have periods of downwelling which would could amount to a heat source during the heating period (Figure 20). Revisiting the heating period, the affect of downwelling does appear

significant, particularly in the later hours of the heating period (Figure 22). However, while the fraction of heating attributable to along-shelf advection appears to have decreased with the addition of the vertical advection, it still accounts for the bulk of the heating.

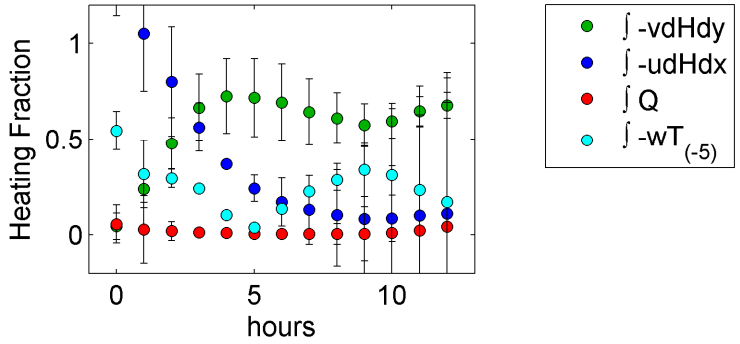

Figure 22: Hourly fraction of integrated term to total observed heating, as in Figure 19 panel B, including the contributions from the vertical advective term.

It is also possible that there are other terms unaccounted for in the heat equation such as turbulent diffusive fluxes. Ramp et al. (2005) has previously suggested diurnal winds in this location were responsible for mixing water column properties and lowering sea surface temperatures. Here we found the percentage of below-critical Richardson numbers also grew in response to the wind, appearing to contrast with Woodson et al (2007) who report the water column remains stable throughout the diurnal wind events. As a whole, Richardson numbers show stability over 90% of the time. Only through separating strong and weak wind days were subcritical Richardson numbers made apparent, and show potential for active mixing through turbulent diffusion. However, considering how well the heat budget is closed by the addition of vertical advection of a reasonable magnitude, the contribution of turbulent mixing is likely to be small.

Future Work

On the mid- and outer-shelf, the dominant cross-shelf balance is between the pressure gradient and the Coriolis forces (geostrophy) (e.g. Lentz et al., 1999). On the inner shelf, other terms in the momentum equation become important as well (Lentz et al., 1999). While we have seen diurnal offshore motions as a result of along-shelf wind-forcing, there are also onshore motions in response to a yet-to-be determined forcing mechanism (Figure 11, panel A). It would be interesting to see how much/if any of the cross-shelf momentum equation is in geostrophic balance at this time scale. Once we understand the role of geostrophy on this inner shelf, a diurnal period momentum budget can be estimated to better understand the contributions of the various terms.

The diurnal heat budget is dominated by 2-dimensional processes. During heating, along-shelf heat gradient advection is the dominant process (2-D in x,y), while during cooling, vertical advection (i.e. upwelling) dominates (2-D in x, z). This means that idealized numerical models can be used to study these processes and try to reproduce these inner-shelf observations. One-dimensional sea breeze-forced numerical simulations produced a large inertial response characteristic of an ocean region far from boundaries. We will try to incorporate an analytical coastal boundary condition (e.g. Craig, 1989) to continue to study 1-dimensional dynamics. The Regional Ocean Model (ROMS) is currently being configured to experiment with a 2-dimensional inner shelf subject to periodic along-shelf sea breeze forcing as in the northern Monterey Bay system. In addition to testing dynamical balances found in this thesis, the numerical model can be used to test the efficiency of setting up cross-shelf Ekman transport as a function of the periodicity of the wind forcing.

Conclusions

The focus of this thesis has been the oceanic response to a strong along-shelf diurnal sea breeze (daily peak of 8 – 14 m/s) in northern Monterey Bay, California. The physical data used to quantify this response included water velocity from acoustic Doppler current profilers, surface gravity wave heights measured acoustically, and temperature from thermistor chain arrays both along- and across- the inner shelf in water depths of 10 – 60 m. This data was part of a larger biophysical experiment to identify physical processes that determine the delivery of invertebrate larvae and juvenile rockfish to rocky intertidal and kelp forest communities in northern Monterey Bay.

Surface gravity wave heights were small during this study (rarely reaching 1.5 m). The measureable Eulerian return flow associated with these waves had a mean of 0.005 m/s, an order of magnitude smaller than diurnal wind-driven flows. However, the time- integrated onshore fluid volume flux due to wave-driven flows is potentially important as it is constant compared to the periodic flux due to wind forcing. Integrated over one day, the onshore transport due to diurnal wind is on the order of 10^4 m^2. In contrast, it would take about four days at the average rate of the observed Stokes' drift flux to transport the same volume of fluid.

The effect of diurnal sea breeze was examined by creating an ensemble average from 45 days when local westerly sea breeze reached a maximum of at least 8 m/s. Hourly values of wind, temperature, and velocity at each level in the water column were averaged in time centered on the peak of the westerly wind. This method worked well to both qualitatively describe the average effect of the sea breeze on the coastal ocean and to give quantitative estimates of diurnal heat exchange.

A heat budget written for a control volume was used to examine and compare the contributions of various terms in the heat equation to the daily heating and cooling cycle. I find 92% ± 13% of the heating signal is explained by along-shelf advection of a heat gradient. The heat gradient arises from the particular location of this study, near

the frontal region separating recently upwelled, cold waters of Pt. Ano Nuevo with warm waters of the Monterey Bay upwelling shadow. Measured along-shelf velocities are predominantly out of the bay and are reversed by diurnal wind. The warming period occurs during the evening relaxation of the wind which results in flow from the shadow towards the upwelling plume, transporting heat down the gradient and warming the water column.

None of the heat equation terms estimated directly from data accounted for the daily cooling period. Both conservation of mass with a two-dimensional coastline and isopycnal displacements yielded estimates of upwelling velocities on the order of 10^{-4} m/s (10 m/day) across a 800 m ± 75 m horizontal plane which closed the heat budget during the cooling period to within 5%, comparable to the confidence with which diurnal heating was closed. Also seen in the average day was an increase of 40% of the number of hourly observations with subcritical Richardson numbers (Ri# < 0.25, indicative of mixing by shear instability in a stratified fluid) in the surface layer. An estimate of the vertical diffusion contribution to the heat budget will be quantified in the future. However, considering how well the heat budget is closed by the addition of vertical advection, the contribution of turbulent mixing is likely small. Thus, as in previous work, sea breeze-driven diurnal upwelling is the primary cause of the observed daily cooling in this location (Woodson et al., 2007).

Measured daily offshore surface transport at 20 m (15 m) depth was 77% ± 12% (36% ± 9%) of the theoretical Ekman transport estimate due to an along-shelf wind. These percentages are within the confidence limits of previous low-frequency inner-shelf observations for this depth (Lentz, 2001; Kirincich et al., 2005). This suggests that the adjustment to a steady Ekman balance is achieved within the diurnal cycle, or that it is more appropriate to compare offshore transports driven by periodic forced oscillations to a different quantity.

In contrast to the regional-scale processes identified in previous coastal circulation studies in Monterey Bay, the inner shelf in the northern part of the Bay is subject to forcing from a wide variety of local physical mechanisms. Thus it is

remarkable that in the diurnal band in northern Monterey Bay we can identify two separate and distinct, essentially two-dimensional processes that dominate the daily addition and removal of heat: along-shelf advection of a temperature gradient during heating and vertical upwelling of cold water during cooling.

Consideration of circulation associated with the two processes dominating the daily heat budget give insight into patterns that have the potential to affect planktonic larvae on this timescale. During the early morning/evening warming period, the system is dominated by advection from the shadow zone towards the upwelling plume. Organisms within the shadow can be transported up the coast with this mechanism. During the afternoon cooling period, cross-shelf circulation associated with upwelling becomes important. Here organisms that maintain their position in the lower water column can be brought onshore to recruit. The biological implications of these findings are a work in progress and will require future interdisciplinary collaboration. It will be interesting to compare the effectiveness of regional versus these localized temperature-gradient and wind-driven mechanisms on determining larval recruitment.

Bibliography

Allen, J.S., P.A. Newberger, and J. Federiuk. “Upwelling Circulation on the Oregon Continental Shelf. Part I: Response to Idealized Forcing.” *Journal of Physical Oceanography* 25.8 (1995): 1843-1866.

Álvarez, O. et al. “A note on sea-breeze-induced seasonal variability in the K1 tidal constants in Cádiz Bay, Spain.” *Estuarine, Coastal and Shelf Science* 58.4 (2003): 805-812.

Austin, Jay A., and Steven J. Lentz. “The Inner Shelf Response to Wind-Driven Upwelling and Downwelling*.” *Journal of Physical Oceanography* 32.7 (2002): 2171-2193.

Banta, Robert M. “Sea Breezes Shallow and Deep on the California Coast.” *Monthly Weather Review* 123.12 (1995): 3614-3622.

Craig, Peter D. “A model of diurnally forced vertical current structure near 30° l atitude.” *Continental Shelf Research* 9.11 (1989): 965-980.

Cushman-Roisin, B. *Introduction to Geophysical Fluid Dynamics, 320 pp*. Prentice-Hall, Upper Saddle River, NJ, 1994.

Dever, E. P., and S. J. Lentz. “Heat and salt balances over the northern California shelf in winter and spring.” *Journal of Geophysical Research* 99.C8: PAGES 16,001–16,017.

Drake, Patrick T., Margaret A. McManus, and Curt D. Storlazzi. “Local wind forcing of the Monterey Bay area inner shelf.” *Continental Shelf Research* 25.3 (2005): 397-417.

Ekman, V. W. “On the influence of the earth’s rotation on ocean currents. Ark. f.” *Mat. Astr. och Fysik., Stockholm* 6.2 (1905): 11.

Emery, W. J., and R. E. Thomson. *Data analysis methods in physical oceanography, 634 pp*. Pergamon, New York, 1998.

Farrell, T. M., D. Bracher, and J. Roughgarden. “Cross-shelf transport causes recruitment to intertidal populations in central California..” *Limnology and Oceanography* 36.2 (1991): 279-288.

Fewings, Melanie, Steven J. Lentz, and Janet Fredericks. “Observations of Cross-Shelf Flow Driven by Cross-Shelf Winds on the Inner Continental Shelf.” *Journal of Physical Oceanography* 38.11 (2008): 2358-2378 .

Gill, A. E. *Atmosphere-Ocean dynamics, 662 pp.* Academic, San Diego, California, 1982.

Graham, W. M., and J. L. Largier. “Upwelling shadows as nearshore retention sites: the example of northern Monterey Bay.” *Continental Shelf Research* 17.5 (1997): 509-532.

Hendrickson, John, and Jamie MacMahan. “Diurnal sea breeze effects on inner-shelf cross-shore exchange.” *Continental Shelf Research* 29.18 (2009): 2195-2206.

Kindle, J. C, R. M Hodur, and others. “A COAMPS™ reanalysis for the Eastern Pacific: Properties of the diurnal sea breeze along the central California coast.” *Geophysical Research Letters* 29.24 (2002): 2203.

Kirincich, A. R. et al. “Wind-driven inner-shelf circulation off central Oregon during summer.” *J. Geophys. Res* 110 (2005).

Kirincich, Anthony R., Steven J. Lentz, and John A. Barth. “Wave-Driven Inner-Shelf Motions on the Oregon Coast*.” *Journal of Physical Oceanography* 39.11 (2009): 2942-2956

Lentz, S. et al. “Momentum balances on the North Carolina inner shelf.” *Journal of Geophysical Research* 104.C8 (1999).

Lentz, S. J. “A heat budget for the northern California shelf during CODE 2.” *Journal of Geophysical Research-Oceans* 92.C13 (1987).

---. “Current dynamics over the northern California inner shelf.” *Journal of Physical Oceanography* 24.12 (1994): 2461-2478.

---. “Sensitivity of the Inner-Shelf Circulation to the Form of the Eddy Viscosity Profile.” *Journal of Physical Oceanography* 25.1 (1995): 19-28.

---. “The Influence of Stratification on the Wind-Driven Cross-Shelf Circulation over the North Carolina Shelf.” *Journal of Physical Oceanography* 31.9 (2001): 2749-2760.

Lerczak, J., M. C. Hendershott, and C. D. Winant. “Observations and modeling of coastal internal waves driven by a diurnal sea breeze.” *Journal of Geophysical Research* (2001).

Madsen, Ole Secher. “A Realistic Model of the Wind-Induced Ekman Boundary Layer.” *Journal of Physical Oceanography* 7.2 (1977): 248-255 .

Mitchum, G. T., and A. J. Clarke. “The frictional nearshore response to forcing by synoptic scale winds.” *Journal of Physical Oceanography* 16.5 (1986): 934-946.

Mooers, C. N. K. “A compilation of observations from moored current meters and thermographs, vol 2: Oregon continental shelf,” August– September 1966, Data Rep. 68-5, Oreg. State Univ., Corvallis. (1968)

Mooers, C. “Several effects of a baroclinic current on the cross-stream propagation of inertial-internal waves.” *Geophysical and Astrophysical Fluid Dynamics* 6 (1975): 245–275.

Paduan, J. D., and L. K. Rosenfeld. “Remotely sensed surface currents in Monterey Bay from shore-based HF radar (Coastal Ocean Dynamics Application Radar).” *J. Geophys. Res* 101.20 (1996): 669–20.

Paduan, J. D., and M. S. Cook. “Mapping surface currents in Monterey Bay with CODAR-type HF radar.” *OCEANOGRAPHY-WASHINGTON DC-OCEANOGRAPHY SOCIETY*- 10 (1997): 49-52.

Petruncio, Emil T., Leslie K. Rosenfeld, and Jeffrey D. Paduan. “Observations of the Internal Tide in Monterey Canyon.” *Journal of Physical Oceanography* 28.10 (1998): 1873-1903.

Ramp, S. R. et al. “Observations of upwelling and relaxation events in the northern Monterey Bay during August 2000.” *J. Geophys. Res* 110 (2005).

Rippeth, Tom P. et al. “Current oscillations in the diurnal-inertial band on the Catalonian shelf in spring.” *Continental Shelf Research* 22.2 (2002): 247-265.

Rosenfeld, L. K. “Diurnal period wind stress and current fluctuations over the continental shelf off northern California.” *J. Geophys. Res* 93 (1988): 2257–2276.

Rosenfeld, L. K. et al. “Bifurcated flow from an upwelling center: a cold water source for Monterey Bay.” *Continental Shelf Research* 14.9 (1994): 931-964.

Rosenfeld, L. K. et al. “Methodology for a regional tidal model evaluation, with application to central California.” *Deep-Sea Research Part II* (2008).

Send, Uwe, Robert C. Beardsley, and Clinton D. Winant. “Relaxation From Upwelling in the Coastal Ocean Dynamics Experiment.” *Journal of Geophysical Research* 92.C2: PAGES 1683–1698.

Storlazzi, C. D., M. A. McManus, and J. D. Figurski. “Long-term, high-frequency current and temperature measurements along central California: insights into upwelling/relaxation and internal waves on the inner shelf.” *Continental Shelf Research* 23.9 (2003): 901-918.

Tilburg, Charles E. “Across-Shelf Transport on a Continental Shelf: Do Across-Shelf Winds Matter?.” *Journal of Physical Oceanography* 33.12 (2003): 2675-2688.

Woodson, C. B., et al. “Local diurnal upwelling driven by sea breezes in northern Monterey Bay.” *Continental Shelf Research* 27.18 (2007): 2289-2302.

Woodson, C. B. et al. “Northern Monterey Bay upwelling shadow front: Observations of a coastally and surface-trapped buoyant plume.” *Journal of Geophysical Research* 114.C12 (2009): C12013.